10-1-2007

High resolution source localization in near field sensor arrays by MVDR technique

Joseph J. Handfield

HIGH RESOLUTION SOURCE LOCALIZATION IN NEAR FIELD SENSOR ARRAYS BY MVDR TECHNIQUE

by

Joseph J. Handfield

B.S. State University of New York at Oswego

(2002)

A thesis submitted in partial fulfillment of the
requirements for the degree of Master of Science
in the Chester F. Carlson Center for Imaging Science
of the College of Science
Rochester Institute of Technology

October 2007

Signature of the Author _____

Accepted by _____
Coordinator, M.S. Degree Program Date

CHESTER F. CARLSON
CENTER FOR IMAGING SCIENCE
COLLEGE OF SCIENCE
ROCHESTER INSTITUTE OF TECHNOLOGY
ROCHESTER, NEW YORK

CERTIFICATE OF APPROVAL

M.S. DEGREE THESIS

The M.S. Degree Thesis of Joseph J. Handfield
has been examined and approved by the
thesis committee as satisfactory for the
thesis requirement for the
Master of Science degree

_____
Dr. Raghuveer M. Rao, Thesis Advisor

_____
Dr. Navalgund A. H. K. Rao

_____
Dr. John Kerekes

_____
Date

THESIS RELEASE PERMISSION

ROCHESTER INSTITUTE OF TECHNOLOGY

COLLEGE OF SCIENCE

CHESTER F. CARLSON

CENTER FOR IMAGING SCIENCE

Title of Thesis:

High Resolution Source Localization in Near-Field Sensor Arrays by MVDR Technique

I, Joseph J. Handfield, hereby grant permission to the Wallace Memorial Library of R.I.T. to reproduce my thesis in whole or in part. Any reproduction will not be for commercial use or profit.

Signature: _____

Date

High Resolution Source Localization in Near-Field Sensor Arrays by MVDR Technique

by

Joseph J. Handfield

Submitted to the
Chester F. Carlson
Center for Imaging Science
College of Science
in partial fulfillment of the requirements
for the Master of Science Degree
at the Rochester Institute of Technology

ABSTRACT

Research over the last decade has led to technological advances in high frequency active and passive detection technology and signal processing. An emerging application area is the standoff detection of concealed objects such as weapons and explosives using penetrating electromagnetic radiation such as terahertz waves (THz). Here sensor arrays are employed in the near field to image the concealed objects. A new approach is investigated to improve upon methods such as Fourier inversion and sum and delay beamforming. A method based on the Minimum Variance Distortionless Response (MVDR) filter technique is developed to localize source points in the electric field coming from a subject. To pinpoint near field sources with precision, this MVDR routine calculates filter responses along a plane that has direction of arrival angle and range axes.

To understand its limitations, this new method is tested for angular resolution in various directions of arrival, ranges, and SNR levels. The results show that this technique has potential to accurately detect closely spaced point sources when only a few sensors are used to collect measurements.

Acknowledgements

I would like to thank the Center for Imaging Science at Rochester Institute of Technology for funding my studies and my stipend as a graduate student. I would also like to thank Dr. Raghuveer M. Rao for his continued guidance, support and enthusiasm over the last year. His advice at all points in this research process always helped me identify problems and regain my focus and concentration when I needed it most. I also appreciate the contributions of my committee members Dr. John Kerekes and Dr. Navalgund Rao. Their help was instrumental toward many reader-friendly revisions of the content of this thesis.

Lastly, I would like to thank my family. Special thanks go out to my loving wife Amy, my wonderful two year old daughter Lilian, Mom, Dad, Grandma and Grandpa Forsythe, and Grandpa Joe Handfield. Each of them has been there for me in one way or another, through good times and bad times alike. I would like to thank them for their continued love and support throughout my undergraduate and graduate college years.

Contents

List of Figures

List of Tables

Chapter 1

Introduction

Security imaging devices have been an area of great interest for the last few decades, especially after an escalation in acts of terrorism involving government buildings and airports. After the events of 9/11/01 in particular, the political and scientific community have been aggressively searching for improvements to security screening measures. There were needs for close range sensing devices similar to walk-through metal detectors and stand-off detectors that could spot threats from secure distances. Concealed Weapon Detection, abbreviated as CWD, is an area of security research that was established to design methods that meet some of these security goals. Over a decade ago, CWD researchers found that terahertz and millimeter wave emissions had the ability to see through nonmetallic and nonpolar solids. Items such as clothing, leather, and plastics that were scanned by a high frequency sensor become partially transparent when imaged by these bands, and if metallic items are concealed, they will reflect high frequency radiation and produce distinct shapes in processed sensor scans (Federeci et al., 2005),(Chen et al., 2005). There is no question that the desire for heightened security after 9/11/01 and technological advances in hardware developments and research have spurred recent growth in CWD.

To further motivate this research, scientists have found several explosive compounds such as RDX, C4, HMX, and TNT have characteristic peaks or features in

their absorption spectrum that will identify these bomb materials on a scanned subject. The spectral peaks are in the range of 0.5-10 Terahertz (THz) and have been commonly found despite the sample's preparation: as grains, powder or mixed in a matrix or container (Federeci et al., 2005). Similar research found that illegal drugs, such as methamphetamine and MDMA can also be recognized by distinct gigahertz (GHz) and THz spectra (Federeci et al., 2005).

The Pacific Northwest National Laboratory was one of the first groups to develop a walk-through active detection millimeter wave scanner for close range CWD. Their portal scanner uses wideband holographic imaging technology that conducts planar or cylindrical scans within seconds (Sheen et al., 2001). The wideband frequencies of 27 – 33 GHz produced higher quality images with increased depth than narrowband CWD scans (Sheen et al., 2001). A company called Safeview commercialized the portal technology and has installed them in several U.S. and international security checkpoints. Field testing is now being performed to confirm its improved reliability and efficiency over metal detectors and other security measures (National Research Council, 2007).

The first conclusive near field results for a THz system were published in 1995 by Hu and Nuss, using an active detection technique called Terahertz Time Domain Spectroscopy, or THz-TDS (Hu and Nuss, 1995). This method created THz backscatter with femtosecond laser pulses that rapidly photo-induce currents upon a THz wave generating switch (Dorney et al., 2000). Dorney et al. coupled THz-TDS with a

Michelson interferometer to enhance the sensitivity in images of microscopic cracks and air bubbles that weaken materials in samples of industrial adhesives, formed plastics and ceramics (Johnson et al., 2000). Later, Zimdars performed high definition 2D scans within 8 minutes using hardware available at the time, but envisioned near video rates as new sensor arrays are developed (D. Zimdars, 2005).

To develop an improved high frequency source field reconstruction algorithm, requirements must be addressed. Since THz wavelengths are less than a millimeter in length, any increases in the imaging aperture size to capture distant sources with the required imaging resolution will force imaged subjects to be in the near field. For example, if a 6 cm object was to be resolved at a frequency of 3 THz from a distance of 25 m, the aperture would need to be 4.2 cm across (Rao and Himed, 2005). This example has requirements that do not satisfy the far field approximation, which is calculated by:

$$D > \frac{2d^2}{\lambda} \qquad (1.1)$$

In this well-known equation variable d is the aperture width, D is the range from the central sensor to the source, and λ is the source wavelength. In addition, the maximum sensing range of some THz and millimeter wave frequencies will also be constrained due to atmospheric attenuation. As a result of these factors, a near field imaging method is needed and a few complications are introduced that invalidate standard far field imaging techniques for uniform linear arrays of sensors.

The focus of the research work underlying this thesis was on the development of a near field source localization method. Many areas of near field and far field imaging analysis were reviewed in this thesis research, specifically interferometry-based methods which contrast the incoming signal between pairs of sensors in a linear sensor array. To understand the workings of a near field algorithm and identify where progress can be made, a previously published least squares algorithm was constructed (Rao and Himed, 2005). An improvement over Rao & Himed's optimization routine was then chosen from the realm of high resolution techniques, such as multiple signal classification (sometimes referred to by its abbreviation, MUSIC) and Auto Regressive methods. Finally, a minimum variance distortionless response (MVDR) beamformer method was chosen and modified to use near-field assumptions. This method was derived from recently published work in source localization and the Capon method. Several experiments were then simulated to test the new method's resolution, noise performance, and efficiency when compared to a simpler Delay and Sum beamformer. The next chapter will provide an overview of several radiative point source measurement methods and their influences on the approach of this thesis.

Chapter 2

Background

In imaging systems, the reconstruction of a source distribution using conventional sensing hardware is an intricate process. To clarify the principles of source reconstruction imaging, an example of a complex source incident upon an observation screen is shown in Figure 2.1. When a diffraction pattern is measured along the sensing line, these methods convert its spatial frequencies into a source distribution estimate. Many imaging methods also simplify the reconstruction for far and near field systems by reconstructing a planar projection of the source distribution, called an 'extended source'. This approach can resolve distant far field objects and also reduce the complexity of items with uneven near field source distributions. To approach the thesis problem, a literature search was conducted into published work that dealt with these specific source distribution reconstruction issues. These areas of interest are discussed in this chapter.

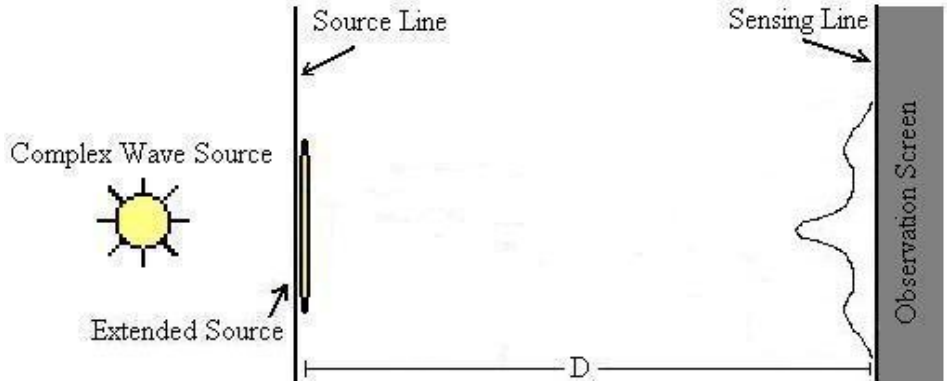

Figure 2.1 – General illustration of complex source distribution upon a sensing line

2.1 Fourier Inversion

In linear shift-invariant imaging systems, the inverse Fourier transform of the far-field correlation is a common method of source distribution reconstruction. Fourier transforms of far field source illumination can reconstruct the spectrum well with standard linear sensor arrays due to the flat planar nature of far field wavefronts. Unfortunately, near-field imaging systems have nonlinear wavefronts so it is difficult to produce images without spherical aberrations. Walsh et al researched near field scanning methods for THz sources that used Fourier inversion techniques and found that spatial modifications were required to transform spherical wavefronts without distortion (Walsh et al., 2004). Fourier methods can commonly produce side lobe artifacts and other noise in the frequency plane that can only be diminished by gathering enough spatial data points on the imaged aperture plane to adequately cover the resulting frequency space. Walsh et al. first suggested transform enhancement strategies such as adding to the number of sensor elements or rotating smaller arrays and then taking multiple measurements to cover the Fourier space well (Walsh et al., 2004). Walsh et al. finally improved the spatial intensity distribution from the interferogram by positioning sensors along curves that match the wavefront's shape. Their simulation results showed that sensors placed along a meniscus that matches a spherical surface works best at modeling the wavefront (Walsh et al., 2004). This can prove to be problematic, since specialized hardware is needed and any significant change in measured range or varied source field

sizes would require repositioning of the sensors along to avoid distortion. It is also uncertain how time consuming this method would be in achieving high resolution.

2.2 The van Cittert-Zernike Theorem

When examining the radiation from a complex source field, interferometry is an effective tool for increasing imaging sensitivity spatially. Spatial coherence in particular is important to this research because it allows one to measure a complex wavefront's shape from the interferogram that a set of radiating sources produces on an observation plane (Hecht 1998). Initial experiments in this field found that source distributions could exhibit some measurable interference while the frequency of the illumination was not 100% coherent. As a result, the term partial coherence was used to classify these situations. In 1938, the van Cittert–Zernike theorem was devised to measure the 'degree of coherence' that two random points in the interferogram have by correlating the composite source field measured at each point. To do this discretely, one must model the source field intensities on an extended projection line that lies parallel to the interferogram, as mentioned in the introduction of this chapter. The projection line, labeled as *source line* in Figure 2.1, can be subdivided into several finite elements of extended sources regardless of their actual position in being in the near field or far field. In theory, each finite element produces a field vibration equal to:

$$\frac{a}{r}e^{jwt-ikr} \qquad where \quad k=\frac{2\pi}{\lambda} \tag{2.1}$$

In equation 2.1, ω is the angular frequency in radians, ***t*** is the elapsed time in seconds, ***r*** is the sensing distance from the element, and '***a***' is a complex random variable that indicates the wavefront's initial amplitude and phase at point P_1 (Zernike, 1990). The overall wave amplitude, or intensity, of *m* electric field measurements upon point P_1 is

$$\mathrm{A}_1 = \sum_m \frac{a_m}{r_{m1}} e^{ikr_{m1}} \tag{2.2}$$

To find the 'likeness' of the measured wavefront at two separate sensing positions P_1 and P_2, as depicted in Figure 2.2, the degree of coherence can be used. Zernike called this expression the 'mutual intensity':

$$J_{12} = \overline{A_1^* A_2} = \sum_m \sum_n \frac{\overline{a_m^* a_n}}{r_{m1} r_{n2}} e^{ik(r_{n2}-r_{m1})} \tag{2.3}$$

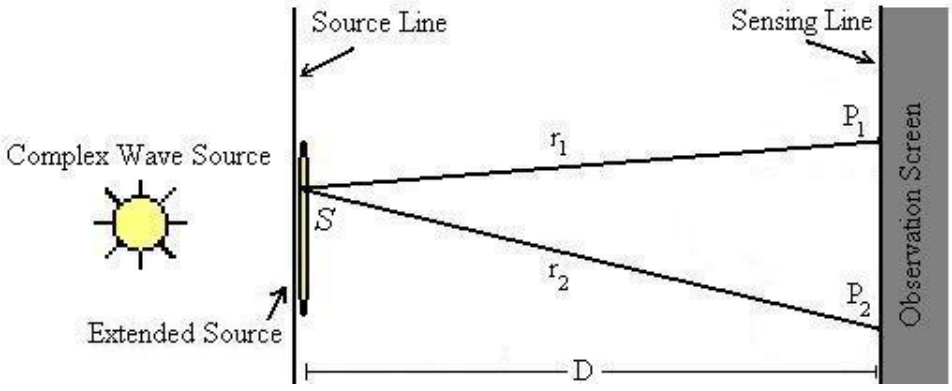

Figure 2.2 – One of 'm' source line measurements to be used in the *degree of coherence* calculation

The bar above the amplitudes in (2.3) indicates the use of their statistical mean amplitude value. Since waves from an illumination source have numerous statistically independent points of origin, they are also spatially uncorrelated (Zernike, 1990). J_{12} then becomes:

$$\overline{a_m^* a_n} = 0 \quad when \quad m \neq n$$

$$J_{12} = \sum_m \frac{\overline{a_m^* a_m}}{r_{m1} r_{m2}} e^{ik(r_{m2} - r_{m1})} \tag{2.4}$$

To calculate the theoretical mutual intensity along the source line, an integral over the extended source is needed (Zernike, 1990). If the position of S in Figure 2.2 was moved across the extended source, the integration variables are the displacements from points P_1 and P_2, noted as x_1 and x_2 respectively. The resulting diagonal distances from P_1 and P_2 to S can then be denoted as r_{x_1} and r_{x_2}, thus making the theoretical mutual intensity:

$$J_{12} = \frac{1}{\lambda} \int \frac{\overline{a^*(x_1) a(x_2)}}{r_{X_1} r_{X_2}} e^{ik(r_{X2} - r_{X1})} dx_1 \, dx_2 \tag{2.5}$$

By means of the coherence method, one can construct distinct intensities of the interferogram for any composite source field. When P_1 and P_2 are close together and the extended source is small when compared to the distance to the observation plane, the degree of coherence equals the normalized Fourier transform of the irradiance distribution across the source (Hecht, 1998). The areas of near field optical coherence tomography and visible band coherence imaging methods have already benefited from

this relationship (Marks et al., 1999). Correlative interferometry, also referred to as sensor interferometry, uses the mutual intensities for all unique pairs of a certain detector or antenna geometry to produce a spectrum. This is a common technique in other areas of research such as radio astronomy (Cohen, 1973). A correlative interferometry source reconstruction method for a uniform linear array signal is analyzed in the next section.

2.3 The Periodogram and Correlative Interferometry

In the search for desirable spatial domain alternatives to the problematic Fourier inversion process, the well established methods of spectral estimation emerged. In order to compute a spectral estimate of an input waveform, the waveform must be sampled over a finite time window as a time function (Kay and Marple, 1981). An ideal spectral estimation technique called the 'periodogram' is a fast Fourier transform estimate that has been used in the past to discretely calculate the power spectral density, or spectrum, of incoming signals. To construct the periodogram, a waveform *x(t)* can be measured at *N* samples per period using summation variable '*n*'. For each sampled frequency, as noted by '*m*', the periodogram is calculated as follows:

$$X_m = \Delta t \sum_{n=0}^{N-1} x_n \, e^{-j2\pi mn/N}$$

$$\varphi_{PER} = \frac{1}{N\Delta t}\left|X_m\right|^2 \qquad for \quad m \in [0, N-1] \qquad (2.6)$$

Kay and Marple indicated that care must be taken in computing the spectrum due to the need to preserve its statistical consistency. Since actual data has random initial phases and some random additive noise over a time interval, the expectation operation needs to be achieved on the sample waveforms by producing correct time averages or ensemble averages (Kay and Marple, 1981). The ideas behind the periodogram can then be applied to a time-sampled spatial correlation estimate. For example, the spatial correlation of two source points can be formed from a slightly modified version of the degree of coherence equation (2.4) as follows:

$$\overset{\Lambda}{R}(y_1, y_2) = \frac{1}{N}\sum_{n=0}^{N-1}\left(\frac{a(x_1)}{r_{11}\lambda} e^{j\omega_0\left(\frac{nT}{N}-\frac{r_{11}\lambda}{c}\right)+j\phi_1} + \frac{a(x_2)}{r_{12}\lambda} e^{j\omega_0\left(\frac{nT}{N}-\frac{r_{12}\lambda}{c}\right)+j\phi_2} \right) \times \left(\frac{a(x_1)}{r_{21}\lambda} e^{j\omega_0\left(\frac{r_{21}\lambda}{c}-\frac{nT}{N}\right)-j\phi_1} + \frac{a(x_2)}{r_{22}\lambda} e^{j\omega_0\left(\frac{r_{22}\lambda}{c}-\frac{nT}{N}\right)-j\phi_2} \right) \quad (2.7)$$

Equation (2.7) calculates the autocorrelation of the sensed field over a linear sensor array. In the calculation, there are N time samples over a period T, and the angular temporal frequency $\omega_o = 2\pi/T$. Since the two source waveforms coming into sensor 1 and 2 have a different incident random phase, ϕ_1 and ϕ_2 are shown outside the complex amplitudes. The source radii, denoted by r in the equation, are given subscripts to indicate the measuring sensor and secondly the source point to which the radii connects, since each will differ significantly in near field analysis. As more source points are added along the source line, polynomial terms will be added to the computed correlation product terms.

Since the autocorrelation of a source distribution from several sensing positions cannot reconstruct an extended source alone, one solution involved the use of an optimization framework. Rao and Himed theorized a least squares solution that reconstructed a projected source distribution as several discrete samples along the source line. The minimum mean squared error between the spatial correlation estimate and the following computed correlation produced their result (Rao and Himed, 2005).

$$g(x,y) \equiv \frac{f(x)f^*(y)}{D^2} \quad where \quad f(x) = \frac{e^{-j\pi\left(\frac{x}{D}\right)^2}}{1+\frac{1}{2}\left(\frac{x}{D}\right)^2} \tag{2.8}$$

In (2.8), x and y are angular displacement distances from a sensor to a source line sample, and D is the distance that a sensor array is separated from a parallel source line, similar to the illustration in Figure 2.2. To fit the least squares analysis, the computed correlation was reformed into a N^2 by k matrix, where k is the number of finite source line samples, and the spatial correlation as a N^2 long column vector. The least squares equation is then:

$$\min(I_k) = \sum_{m=1}^{N}\sum_{n=1}^{N}\left|\hat{R}(y_m, y_n) - \sum_{k=1}^{M} I_k g(y_m - x_k, y_n - x_k)\right|^2 \tag{2.9}$$

The least squares solution vector I_k is the intensities along the source line at evenly spaced source line positions (x_k) in the sensor array's field of view. To produce realistic solutions, the least squares method is then computationally limited to being nonnegative and within the boundary of the source line width that is being measured.

2.4 Capon Beamforming

After using correlation-dependent equations to measure the simulated electric fields in this thesis work, more detail about the near-field signals is desirable. The best way to quantitatively examine the location and intensity of near-field sources is by employing spectrum analysis techniques. In spectrum analysis, the spatial sensor data is transformed into a spectrum of its frequency components. These components have significant traits in their magnitudes, phases and characteristic frequencies that can be used to identify the sources that are being imaged. When significant source distribution data is known, such as the field of view that they reside in, their approximate range, and their peak spectral frequencies, high resolution techniques can be used.

High resolution techniques can consist of many different formulations, but they all generate a spectral estimate of the gathered source data and improve the resolution and detectability by way of filtering, statistical data, or other means. Beamforming methods are generally known as FIR filtering techniques which use multiple frequency steering vectors to align the signal with a certain azimuth angle, commonly called the direction of arrival (DOA). The steering vector is an array of bandpass filters that boosts the frequencies relative to a desired DOA. Nikias and Mendel remarked that Capon's beamformer was 'one of the most popular and important beamformers' and it 'has been the starting point for both signal enhancement and high-resolution DOA estimation' (Nikias and Mendel, 1993).

To use Capon's method, a spatial correlation estimate must be calculated to optimize this filter. Assume matrix R is an N x N spatial correlation of the detected field:

$$R = E\left\{x \cdot x^H\right\} \tag{2.10}$$

where superscript H distinguishes the use of the Hermetian, or complex transpose of the far field signal vector x. The Capon method then evaluates a set of spectra from the signal vector that are the result of a criterion being met (Stoica and Moses, 1997):

$$\min\ h^H R h \quad subject\ to \quad h \cdot a(\theta) = 1 \tag{2.11}$$

In (11), the steering vector $a(\theta)$ is a series of phase delays made for a sensor spacing d:

$$a(\theta) = \begin{bmatrix} 1 & e^{-j\sigma} & e^{-j2\sigma} & \dots & e^{-jm\sigma} \end{bmatrix}^T \qquad where \quad \sigma = 2\pi \frac{d}{\lambda} \sin(\theta) \tag{2.12}$$

The Power Spectral Density, or PSD, of the Capon method has been used in several journal articles to solve the optimization problem (2.11). The PSD is denoted by P_{Capon} below. A particular solution to (2.11) involves applying a finite impulse response (FIR) distortionless filter h_θ to a sample signal vector x to form X_{Capon} as shown below:

$$P_{Capon} = \left(a^H(\theta)\, R^{-1}\, a(\theta)\right)^{-1} \tag{2.13}$$

$$h_\theta = R^{-1} a(\theta) P_{Capon} \qquad X_{Capon} = x^H h_\theta \tag{2.14}$$

When using standard Capon beamforming, the filter selects weights that minimize the output power of the filter to ensure minimal distortion of the narrowband signal of

interest (Jiang et al., 2003). By consistently incrementing the value of θ in the steering vector array, filter responses as shown by either equation (2.13) or (2.14) can be plotted and assessed for a series of DOA angles in the field of view. If any steering method like this is used, very specific and detailed information is needed to construct an effective array steering vector. Source steering angles, array geometry, and receiver responses affect the accuracy of steering vectors, so a sufficient knowledge of incident radiation is critical to the Capon MVDR process (Nikias and Mendel, 1993).

This method has also been called the minimum variance distortionless response (MVDR) beamformer because it can perform well at identifying many signal component peaks by minimizing the variance in the solution weights, producing suitable results with signals traveling at any speed that may have good or poor SNR. It was first used by Capon to spectrally pinpoint centers of activity from seismic sensor data taken by the large aperture seismic array, or *LASA*, in eastern Montana (Capon, 1969). He went on to show that the optimizing ability of the frequency windows used outperformed traditional methods and pointed out the potential use of the method in radio astronomy.

2.4 Source Localization

Similar to MVDR, source localization methods attempt to identify the origination of complex field sources from the recorded sensor array signals. These methods have been applied to radar, sonar, radio astronomy, oceanography, geophysics, seismology,

and robotics in the past (Grosicki et al., 2005). To measure the field along a 2p+1 sensor ULA as a function of time in near-field, consider the geometry in Figure 2.3.

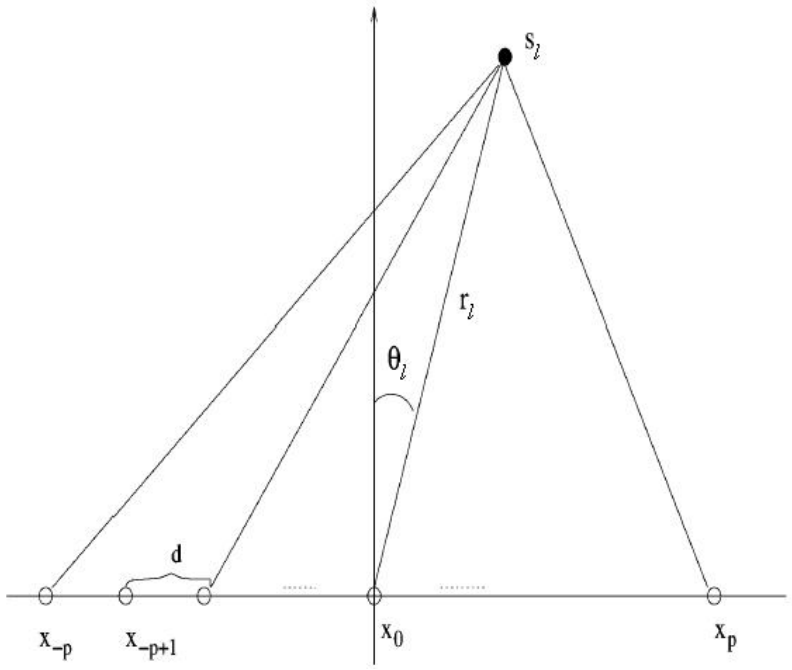

Figure 2.3 – Helpful illustration for source localization with a 2p+1 sensor array

Using the illustration, the field at array indexes $-p \le k \le p$ is (Grosicki et al., 2005):

$$x_k(t) = \sum_{l=1}^{m} s_l(t) e^{j\tau_{kl}} + w_k(t) \qquad (2.15)$$

where $s_l(t)$ represents the lth source signal of m additive sources and $w_k(t)$ is a zero mean complex Gaussian random noise matrix. For a unique solution, Grosicki also assumes that $m \le p$, and that τ_{kl} is the source signal delay between the central sensor '0' and sensor k:

$$\tau_{kl} = \frac{2\pi r_l}{\lambda}\left(\sqrt{1+\left(\frac{kd}{r_l}\right)^2 + \frac{2kd\sin\theta_l}{r_l}} - 1\right) \qquad (2.16)$$

r_l and θ_l are the range and angle parameters of source l, and d is the sensor separation along the array. Since the delay term is difficult to resolve as the square root of a quadratic polynomial, a Fresnel approximation of the field's phase delay across the sensors was suggested (Grosicki et al., 2005). The approximation below can replace τ_{kl} with a second order Taylor expansion, allowing efficient localization by several methods.

$$x_k(t) = \sum_{l=1}^{m} s_l(t) e^{j(\omega k + \phi k^2)} + w_k(t) \tag{2.17}$$

$$\textit{where} \quad \omega = -2\pi \frac{d}{\lambda} \sin\theta_l \qquad \textit{and} \qquad \phi = \frac{\pi d^2}{\lambda r_l} \cos^2\theta_l \tag{2.18}$$

Grosicki et al. suggested solving for the possible binomial exponents of each individual field source by isolating coefficients of the spatial correlation that would allow solutions for each of the quadratic terms. Two solution approaches were proposed: use a subspace-based high resolution estimate, or proceed as the authors did by applying a weighted linear prediction criterion using a polynomial filter (Grosicki et al., 2005). This filter isolates coefficients from the correlation matrix that can be used to derive the unknown sources in the signal. The successful use of a Fresnel approximation to describe a random source field proved a Taylor expansion to be ideal for near field scanning technology, thereby inspiring the approach of this thesis.

Source localization techniques have been used to identify data in speech recognition, communication, radar, and sonar research (Grosicki et al., 2005). These areas have also been explored by many MVDR-influenced beamforming methods

(Vaidyanathan and Buckley, 1995). Research in near field source localization has previously benefited by merging aspects beamforming and steering methods together, showing potential for pairing the methods in this research. Chen et al. performed wideband near field source localization by initially transforming some sample wideband signal data into the frequency domain and separating it into several narrowband frequency bins. They then used a Capon-influenced maximum likelihood criterion on each binned signal to localize the sources (Chen et al., 2002). The paper indicated that this work was based on sensing complex near field acoustic or seismic wave sources. Another research paper (Arceo-Olague et al., 2006) went into detail about efficiency in a near field DOA estimation method called the unconditional maximum likelihood (UML) approach. Their improvement on MVDR and similar techniques involved minimizing a negative log-likelihood function to create the maximum likelihood of the signal. Their UML estimation function outperformed a MUSIC algorithm in root mean square error (RMSE) analysis of angular separation estimation along the range of 5 - 11°, when averaging 1000 samples (Arceo-Olague, 2006). The MUSIC algorithm had much higher RMSE and wider range, for example, when a signal with SNR=11dB was used, it resulted in a 25° error for 5° of separation, to 0.25° error at 11° separation, and SNR values of 9dB-0dB performed worse. The UML function achieved a RMSE range of 0.41° - 0.22° for the same angular separations when SNR values of 11dB – 0dB were plotted. When the algorithms were reused with 500 samples, similar behavior was noticed in UML data, and the MUSIC algorithm performed worse (Arceo-Olague, 2006).

Chapter 3

Approach

The goals of this research were to develop a technique for near field source localization that could be used in terahertz or millimeter wave security scanning, and to evaluate its strengths and limitations. To understand the needs of such a system, a correlative interferometry algorithm was generated from a previously published paper (Rao and Himed, 2005). The resulting program provided insight into the reconstruction of source distributions from their incident radiation without the use of Fourier Transform techniques. The performance of the Rao-Himed routine's simulations then pointed out efficient and sub-par imaging algorithm qualities. These developments and a desire to enhance the sensing ability of near field sources inspired the high resolution technique approach of this thesis. As a result of this progressive research, a superior source distribution analysis method was derived that merged the MVDR method and Source Localization, as shown in the following sections.

3.1 Correlative Interferometry Method Results

In the background section of this thesis, equations 2.7 through 2.9 showed in detail how an accurate 1D reconstruction of a simulated source field can be produced from Rao and Himed's method. An implementation of their method in MATLAB

requires several parameters: the distance between source line and center sensor (D), the number of sensors (N) and sensor element width, the number of finite source reconstruction points (k), the placement of example field points on the source line (x_k), the signal-to-noise ratio (SNR), and the input frequency. Once the sensor size and the desired source line reconstruction points are listed by the user, the program can then simulate the spatial correlation as an ensemble average of several sample records, and the computed correlation (2.8) for all source points. As a result of the calculations, resolution accuracy of an optimized reconstruction can only be possible if the computed correlation matrix is full rank. Here, the rank of a matrix is the number of linearly independent rows or columns it has, and full rank certifies that the rank is equal to the shortest dimension of the matrix. To test the Rao-Himed method while ensuring accuracy in spatial reconstructions, its factors were tested while using a full rank correlation matrix.

Several sets of narrowband test source simulations at a frequency of 1 THz were then used to verify the algorithm's source line signal reconstruction accuracy. These simulation inputs consisted of a source point pair with unit amplitude that was separated along the source line by several wavelengths. The reconstruction points selected for these input signals then occupy a field of view that reaches beyond the source point positions. In this way, accurate reconstruction of the source point pair can be verified while other sample reconstruction points around the source points remain zero.

This resolution accuracy technique was first applied to variations in sensor element size. An initial result of the measurement process identified that the Rao-Himed

method had a maximum range limitation for each number of samples taken, where surpassing the range degraded the reconstruction and correlation matrix rank. As the number of reconstruction samples was increased, the max range decreased exponentially. Also, the maximum range required for resolution accuracy of a 6λ wide array did not change significantly as sensor elements were decreased to smaller than ⅓ λ.

A second test observed the range limitation of a 6λ wide 19 sensor array as an effect of the sampling distance intervals. Initial simulations that sampled the source line reconstruction at increments of less than λ shortened the maximum range for accurate sample resolution significantly. An exponential increase in the number of ensemble average records was also needed to minimize reconstruction mean square errors below 10% in these simulations, suggesting that sampling point sources at under λ intervals is not practical for this method. Finally, a separated source point pair was simulated for increasing amounts of samples and decreasing maximum range, as mentioned in the previous paragraph. The reconstruction samples were taken in intervals of λ and 2λ. The 2λ intervals produced a 50% larger maximum range, as shown in Figure 3.1, while maintaining accurate reconstruction resolution.

A third test simulation was then devised to identify the change in the maximum range limitation as the sensor array width was varied from 10 sensors (3λ) to 19 sensors (6λ). This resulted in an average accurate resolution range increase of 21%. To enhance the possible accurate resolution range of the 6λ array by 50%, similar to the results in 3.1, a 100 sensor (33λ width) array is needed. This information is also plotted in Figure 3.2.

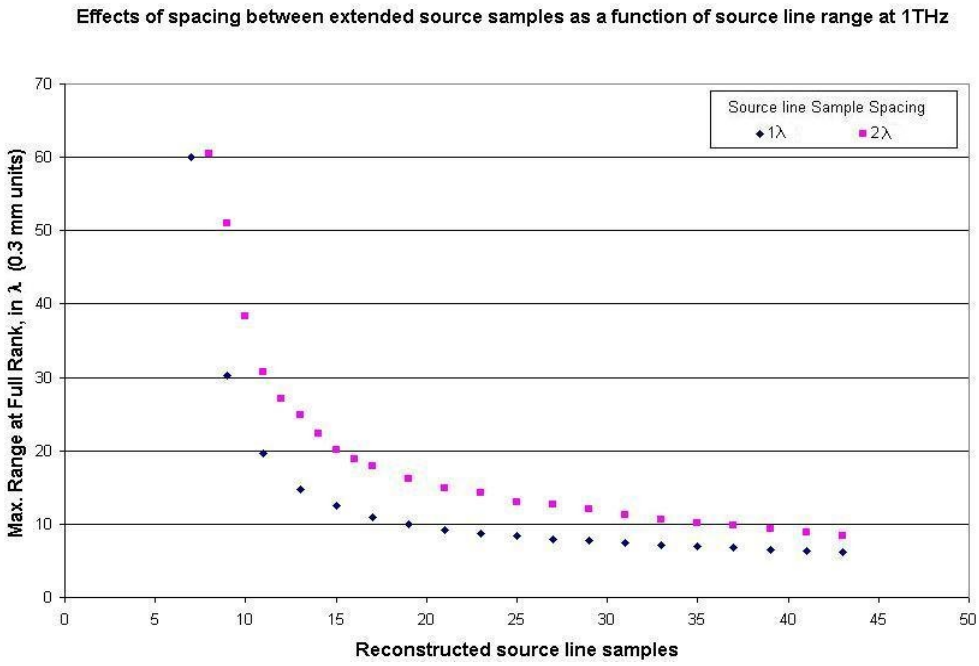

Figure 3.1 - Plot of maximum source line range in λ for accurate resolution versus number of source samples being reconstructed. The data sets show results of doubling the separation between samples.

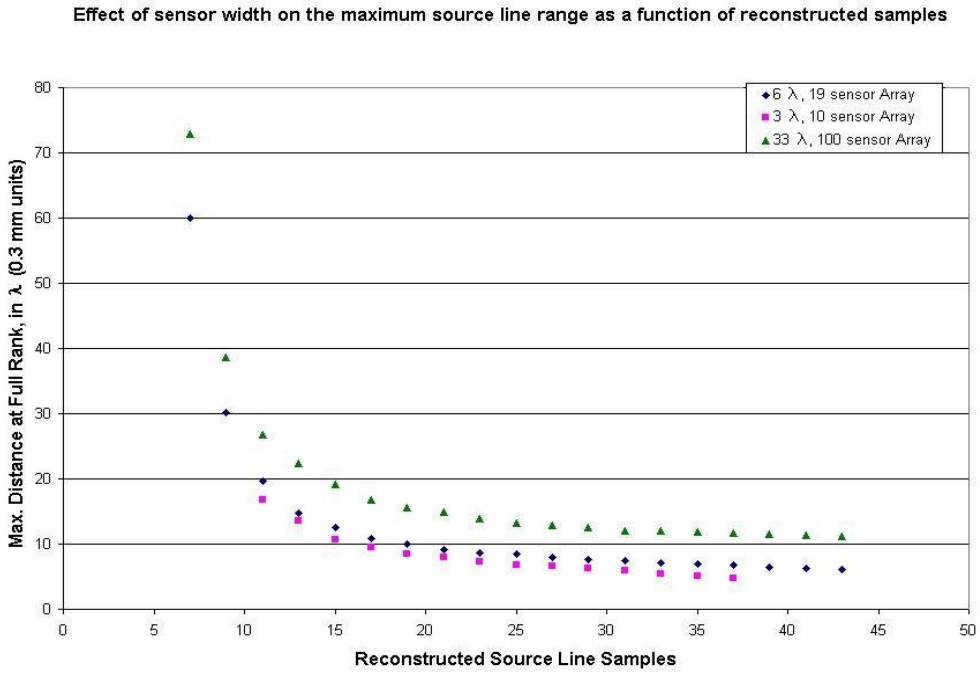

Figure 3.2- The effects of increasing the linear array width using the same criteria as Figure 3.1

Further results concluded a few performance issues with the least squares method, particularly that hundreds sample measurements are needed to create an accurate ensemble average of distributions with more than two separated sources. A much larger sensor array is also needed in order to get quality imaging scans by this method alone. The implementation of this method allowed insight toward desirable characteristics in a near field imaging method, such as variability in range and the field of view, and quality resolution. The attempt of this thesis approach is to improve these factors measurably.

3.2 Derivation of a Near Field MVDR Filter

A better understanding of the near field imaging methods and high resolution spectral estimation methods was required to improve results. Standard Capon beamforming, as discussed earlier, is strictly for far field signals because the wavefronts are assumed to be planar in equations (2.10) through (2.14). To consider a Capon-type method's potential in the near field required localizing waves with curved wavefronts, using phase delays that are a function of both range and DOA. This can be achieved by creating steering vectors with a Fresnel phase delay. The equation for a near field steering vector shown below was borrowed from an earlier mentioned research paper on unconditional maximum likelihood estimation (Arceo-Olague, 2006). The delay terms in the vector can be constructed using the Taylor expansion shown in (2.17) and the definitions of ω and ϕ from (2.18). If the sensors in the interferometric array are indexed for all k in $-p \leq k \leq p$, the steering vector becomes

$$a(\theta_l, r_l) = \left[e^{-j(p^2\phi - p\omega)} \quad \dots \quad e^{-j(\phi-\omega)} \quad 1 \quad e^{-j(\phi+\omega)} \quad \dots \quad e^{-j(p^2\phi + p\omega)} \right] \tag{3.1}$$

$$\textit{where} \quad \omega = -2\pi \frac{d}{\lambda} \sin\theta_l \qquad \textit{and} \qquad \phi = \frac{\pi d^2}{\lambda r_l} \cos^2\theta_l$$

Using this innovative steering vector, the Capon MVDR method can then be revamped as a function of two parameters, as shown in this modified derivation

$$\min h_{\theta,r}{}^H R\, h_{\theta,r} \quad \textit{subject to} \quad h_{\theta,r} \cdot a(\theta_l, r_l) = 1 \tag{3.2}$$

$$P_{Capon} = \left(a^H(\theta_l, r_l)\, R^{-1}\, a(\theta_l, r_l) \right)^{-1} \tag{3.3}$$

$$h_{\theta,r} = R^{-1} a(\theta_l, r_l) P_{Capon} \qquad X_{Capon} = x^H h_{\theta,r} \tag{3.4}$$

The power spectral density, calculated by equation (3.3), can be used as a general solution to localize a near field source distribution, or equation (3.4) can be used to produce the output of an MVDR filter and a certain signal of interest, X_{Capon}. Equations (3.1) through (3.4) are functions of the angle θ_l which can be replaced by a series of distinct DOA values in a predetermined aperture or field of view. The range r_l in the ϕ term can then be incremented over several MVDR iterations to perceive depth of the sources that impinge on the detecting array from significant DOA. The resulting filter responses give the user a set of spectral intensities for all (r_l , θ_l) pairs in the field of view of the sensor array, as illustrated in Figure 3.3. Depending on the desired sampling rate of r_l and θ_l , and the ideal field of view size needed for certain targets, the scanned area can be manipulated to the desired dimensions of the user of this MVDR routine.

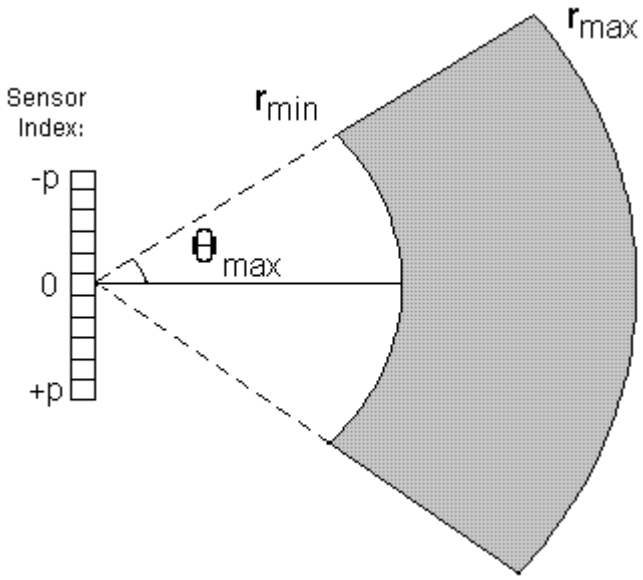

Figure 3.3 – Geometry of a modified Capon MVDR method scan that uses Fresnel-influenced delays

To model actual fields that would impinge on a sensor array, equations (2.17) and (2.18) are used to create a test signal. Time averaging at a user defined sampling interval is then needed to treat the signal vector as a function of time, as shown in the periodogram spectral estimator. The following equation simulates an actual signal record:

$$X_{\Phi}(t) = \sum_{l=1}^{m} s_l \, e^{j\left(\omega k + \phi k^2\right)} e^{j2\pi \frac{n\Delta t}{T}} \, e^{j\Phi_l} + W_k(t) \qquad (3.5)$$

The signal record in (3.5) is obtained over $2p+1$ sensors where k is the sensor position within $-p \le k \le p$. The second exponential term ensures that the signal is measured at $T/\Delta t$ samples per period. The algorithm will calculate this in matrix fashion, and ensure that random Gaussian noise matrix $W_k(t)$ is the same size as the number of sensors -by- the number of samples. Since one random phased sample of the signal vector will produce a

correlation with limited accuracy, the equivalent to the use of the expectation operator on a correlation estimate is needed. This can be achieved by ensemble averaging several signal record samples with random incident phases applied to each simulated source. To calculate the correlation of one random phase record using a signal record as shown in (3.5), the following matrix product is needed:

$$\hat{R}_{\Phi} = \frac{\Delta t}{T} X_{\Phi} X_{\Phi}^{H} \tag{3.6}$$

Equation (3.6) will perform a time average as the signal matrix is spatially autocorrelated, since $\Delta t/T$ is the inverse of the number of time samples. When a desired number of random phased signal records is obtained using (3.5), a correlation estimate can be obtained by averaging the correlations from each record. As the number of records used is increased to achieve similar results to an expectation, the resolution of the MVDR method is expected to increase. Once a correlation of desired accuracy is computed, the algorithm requires several inputs:

- DOA, to establish the center of the field of view if larger DOA values are required
- The perpendicular distance from the sensor to source line (minimum range)
    - The range can be incremented smaller or larger as needed in the algorithm if the range sampling is not sufficient for peak detection in previous runs.
- The width of the field of view, which then passes the minimum and maximum DOA angles to be used into the algorithm

- The SNR of simulated noise for the test signal, if needed
- The distance increment to be used when subdividing the field of view

To decode the detected field into individual source field points, equation (3.1) can be used to compute a steering vector for every unique (r_l , θ_l) pair that can then produce output spectra for each vector used. Each steering vector is then combined with the spatial correlation of the detected field using equations (2.13) and (2.14) to produce spectra. The spectra are collected in a '*Range-DOA-space*' matrix. Automatic detection techniques or having a technician examine a 3-dimensional mesh plot of the complete matrix can then be used to identify signal component peaks.

The idea of using a superresolution technique to scan across a target plane can be found in some Synthetic Aperture Imaging work as well. Benitz developed a technique called *High-Definition Vector Imaging* (HDVI) which scanned a plane across the ground using range and cross-range axes. Using techniques based on Capon's method and MUSIC, he identified distant trucks and other vehicles in a forested area from overhead radar scans (Benitz, 1997). The results of this study showed lower false alarm rates, increased resolution, and reduced sidelobes, clutter and speckle (Benitz, 1997). The Fresnel-Capon-Type method should have analogous benefits to the HDVI method, as shown by our results which are discussed in the next chapter.

Chapter 4

Research Results

To determine the usefulness of the near field MVDR algorithm, an investigation into its abilities and limitations is needed. A MATLAB algorithm was generated using three functions: a sample signal generator that gathered several input values, a MVDR filtering function, and a SNR function that generated random complex Gaussian noise. To test the abilities of the newly-derived two parameter MVDR method in the near field, a series of experiments were simulated. The MVDR source code is posted in Appendix 3.

4.1 Experimental Setup

The data sets that are discussed in these research results are gathered from several simulations. The sensor arrays are assumed to have an inter-element spacing d equal to $\lambda/4$, to avoid ambiguity in sensor measurements of a source with wavelength λ. The size of the sensor will be discussed in each experiment, since sensors with different amounts of elements will be simulated. The signals used in each of the experiments will consist of a pair of point sources that are located at the same range from the center sensor of the measuring array but separated in angle as shown in Figure 4.1. A field of view is then measured using the 2D scanning technique mentioned in the Approach, and pictured in Figure 3.3. The resulting MVDR filter responses for each range and DOA intersection can then be plotted as a contour plot or mesh plot to examine the spatial frequency peaks.

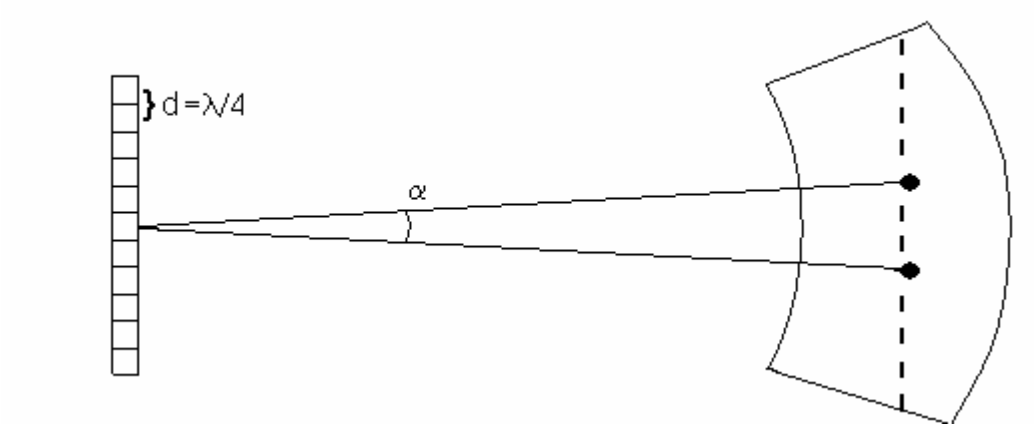

Figure 4.1- Sensor array angular resolution of a pair of point sources, noted by the angle α

To have accurate resolution in angle and range, the resulting spectral peaks will have a crest that is located in the correct spatial frequency position of the contour or mesh plot. If the source pair simulation parameters are manipulated to place the sources closer and closer, eventually the peaks of each source will start to converge, creating noise and incorrect spatial frequency peak positions. Minimum angular resolution data was then taken from the smallest clear angular separation, and care was taken in visually confirming this data at all values in each experiment in the same manner. In the future, a peak identification routine can be written to confirm the resolution as well. To supplement this discussion, a contour showing acceptable resolution and poor resolution status can be seen in Figure 4.2. The poor resolution example has multiple noisy spiked peaks about the actual DOA and range positions of the input simulated source point pair. Since the DOA and Range positioning of the crest of each peak should correspond to the input source pair parameters, this fact becomes the most important resolution criterion.

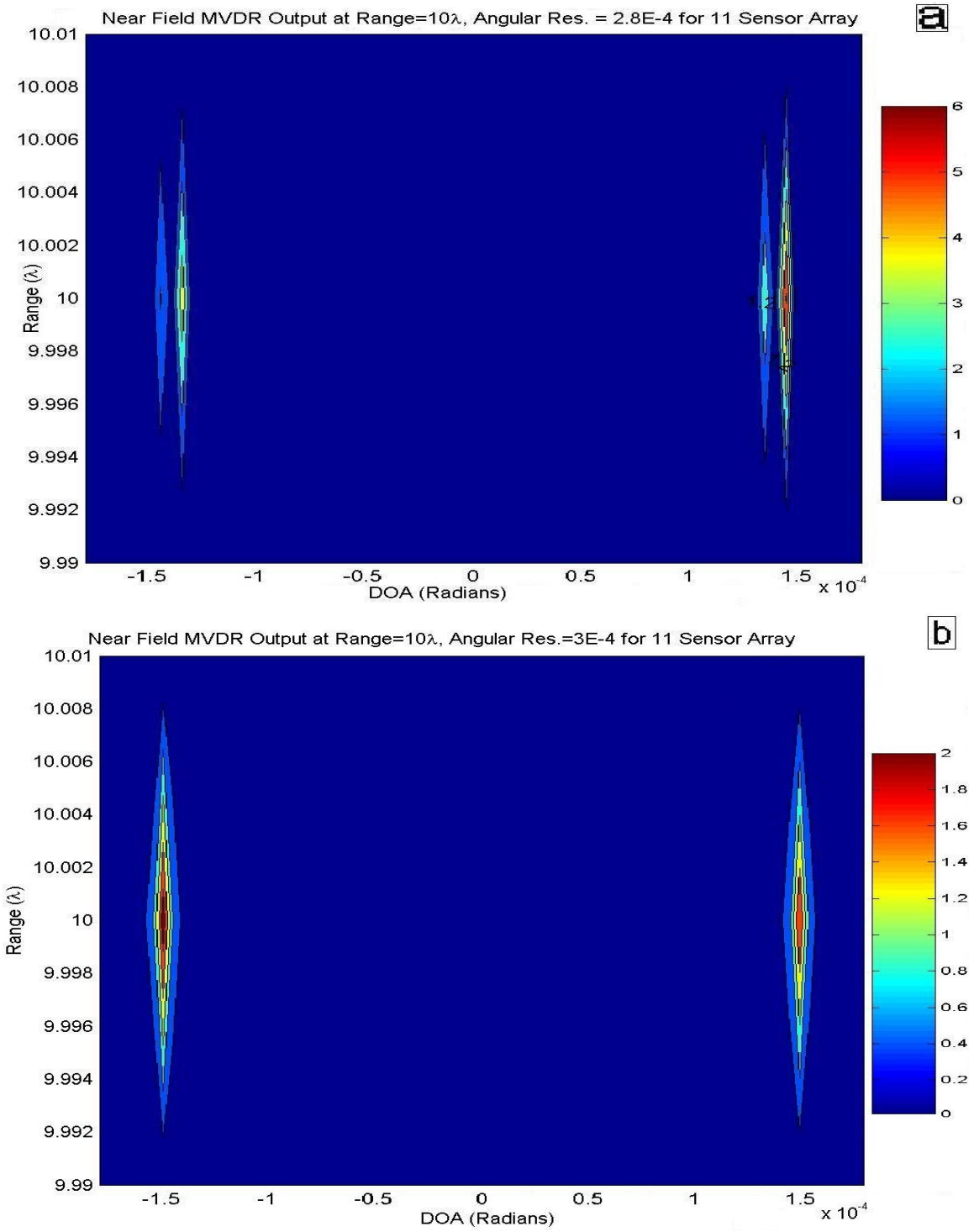

Figure 4.2 – Contour Plots of Near Field MVDR with poor resolution (a) and good resolution (b)

The resolution measurements in the following research are gathered using these inferences. In order to achieve these results, the near field MVDR signal correlation input is created using ensemble averages of many random initial phase signal records and periodic time averages, as mentioned in the derivation.

4.2 Experiment 1

The two parameter MVDR algorithm was first tested for imaging resolution of a source point pair as a function of mean DOA and sensing distance. To measure the effects of these factors alone, a signal correlation was simulated from 150 noiseless signal records. The minimum angular resolution was plotted at multiple range distances that incremented between 1λ and 12λ, to keep within the far field approximation for an 11 sensor array with λ/4 interelement spacing. The minimum angular resolution between source point pairs for varying range measurements was then generated for several mean DOA: broadside (0° for this data), +10°, +20°, +30°, and +40°. A plot of resolution results for each of the signals is posted in Figure 4.2. The angular resolution measurements have an overall range of 2.5–3.6 $\times 10^{-4}$ radians, showing no significant variations. It is valid to say that the angular resolution of this method should be quite uniform over a wide field of view at any DOA or fixed range. This positive attribute makes this method much more useful than an imaging technique that suffers from resolution inconsistency at larger ranges or wide angles.

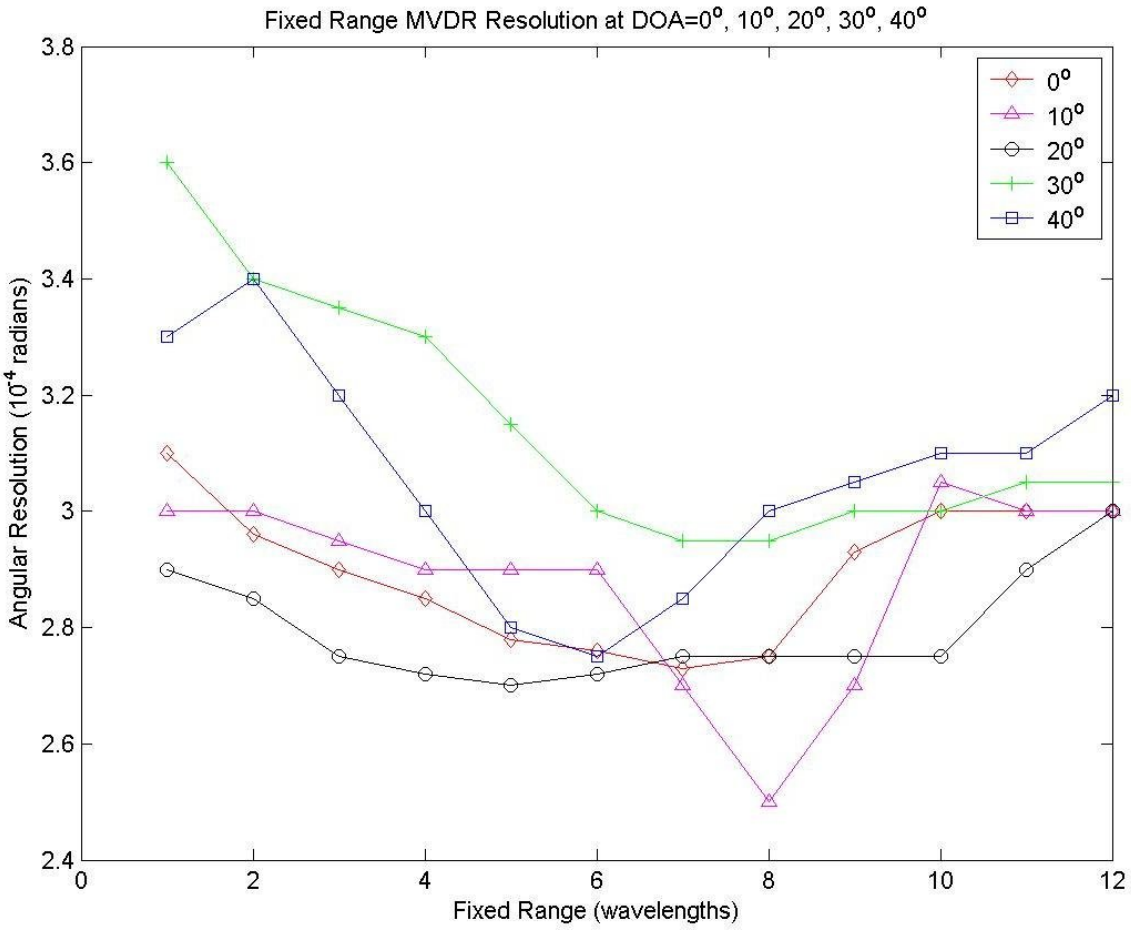

Figure 4.3 – Source pair resolution at several fixed range distances for a series of DOAs.

4.3 Experiment 2

This next experiment was conducted with a noiseless signal and 20 signal records to estimate the improvement in angular resolution by doubling the sensor array length. A plot in Figure 4.3 provides a resolution comparison of the 11 sensor array with 2.5λ effective length and a 21 sensor array with 5λ length at broadside (DOA = 0°). The plot

indicated that angular resolution is almost 50% better on average for the larger sensor array. Since a much larger sensor than these is needed for CWD in the near field, it can be concluded that resolution will not be an issue over these longer ranges.

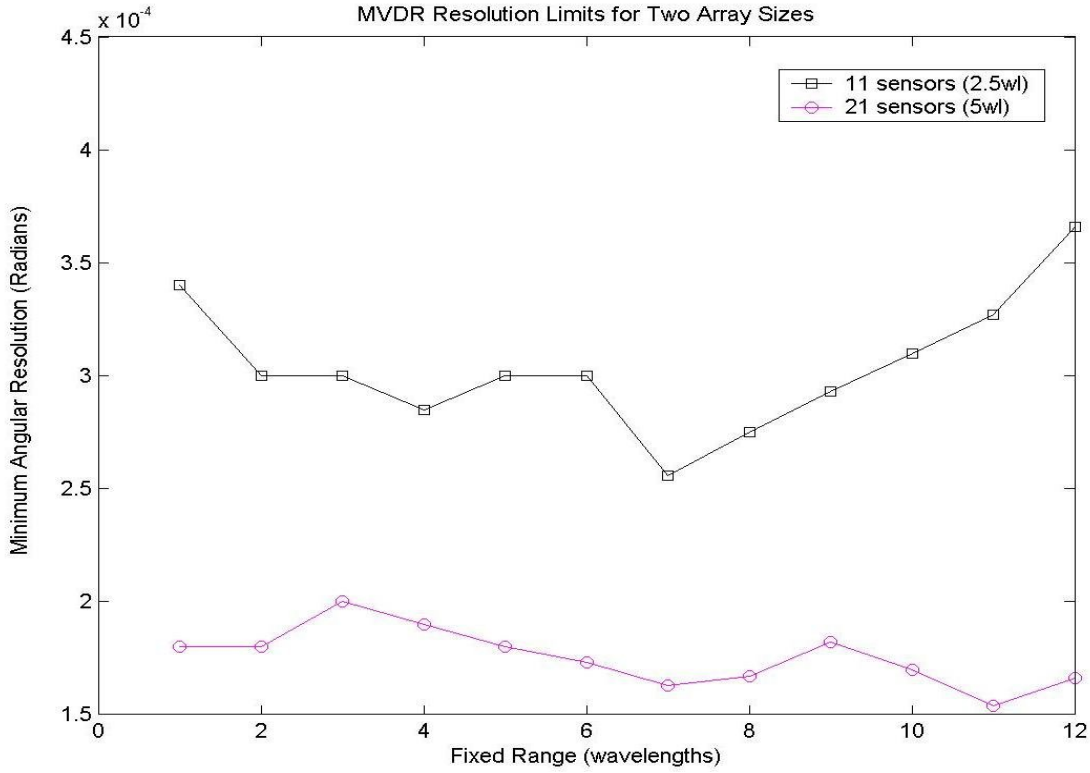

Figure 4.4 – MVDR method angular resolution as a function of array length, at a broadside DOA

4.4 Experiment 3

To estimate the performance in noise using the same approach as previously noted, another experiment was simulated. Initial results were attempted by averaging 20 sample records with the same 11 sensor array with $\lambda/4$ sensor separation that was

simulated for previous results. Source point pairs located at a mean DOA of broadside and fixed range of 10λ were then resolved at various SNR values. These minimum angular resolution measurements are plotted for analysis in Figure 4.4.

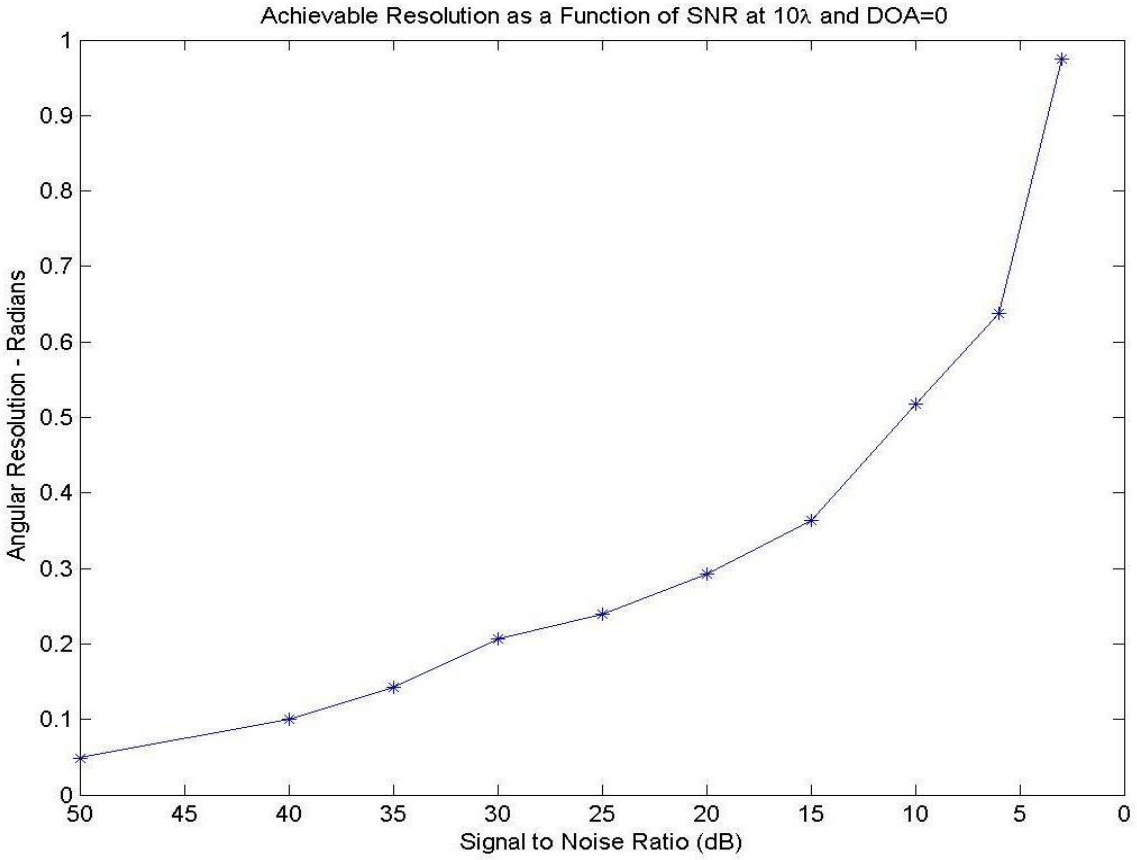

Figure 4.5 – Minimum angular resolution vs. SNR of spectral peaks for 20 averaged records

The y-axis range of the plot in Figure 4.4 corresponds to angular resolution of 2.8° at 50dB and 55.85° at 3dB, which is not particularly reasonable. The resolution plots revealed a second issue as well, a flattening of the spectral peaks across their range axes. Once these spatial frequency peaks became plateau shaped due to the noise, the range

component of the peak was hard to identify when checking simulation results. This occurred particularly in plots as the SNR was increased past 40dB, so an increase to 60 records was used to take better source range measurements at 3dB. The range was varied from 10λ to 1λ for a few measurements to see if proximity to the sensor array could increase range resolution. Figure 4.5 is a plot of the pair of spectral peaks identified by the MVDR filter, and Figure 4.6 shows improvement in range detection for the 1λ data.

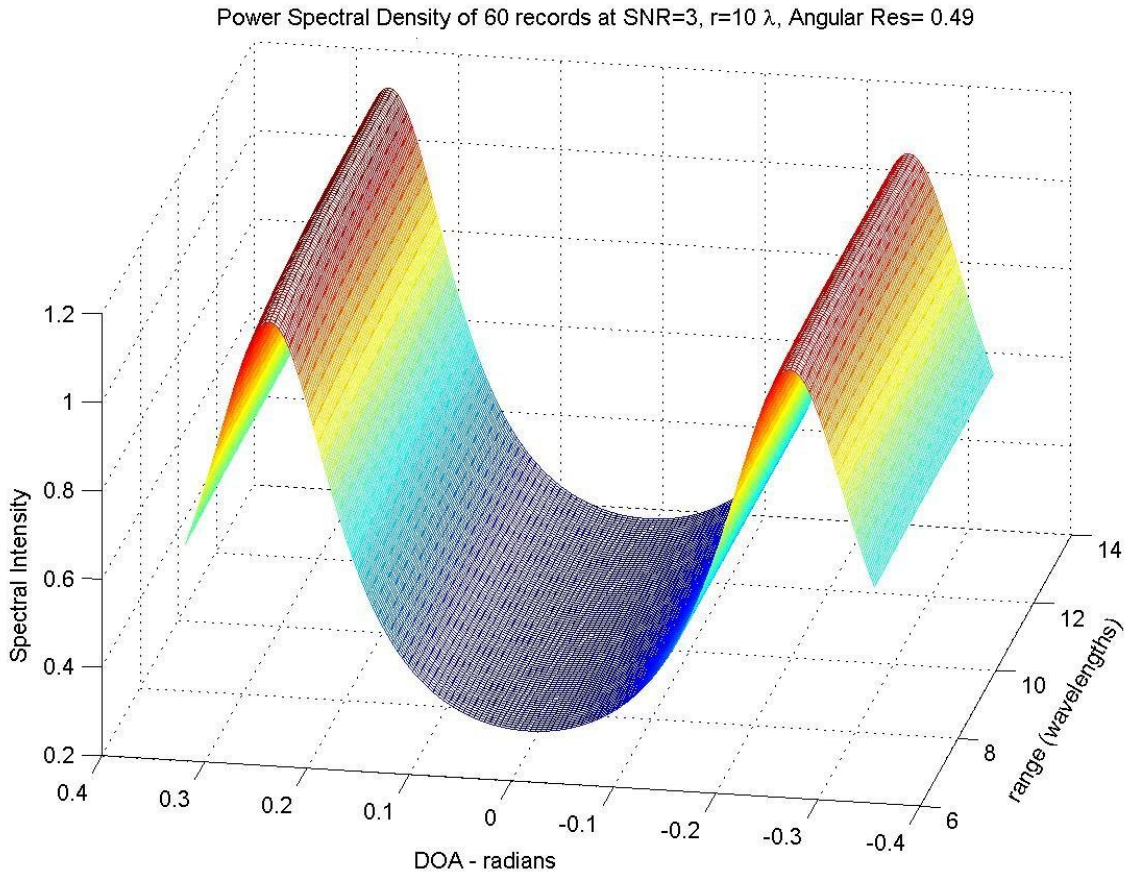

Figure 4.6 – Angular resolution measurement taken at 10λ with 60 records

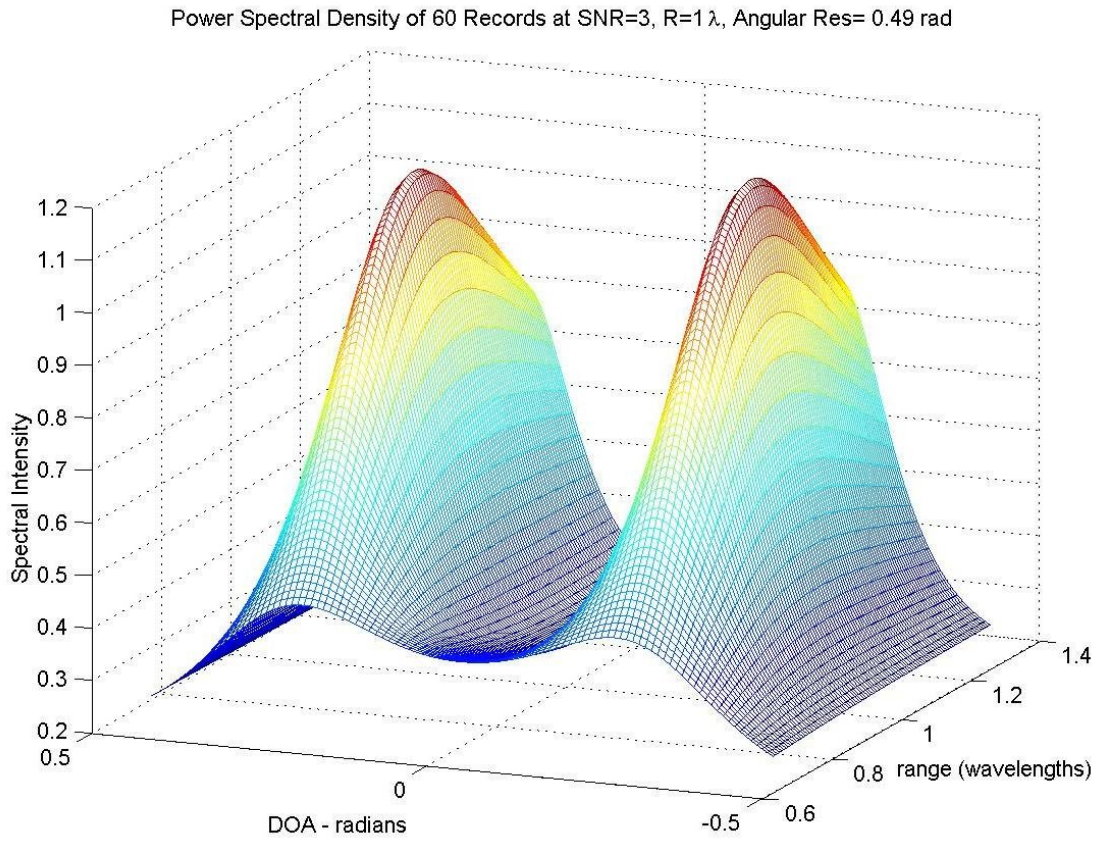

Figure 4.7 – Angular resolution measurement taken at 1λ with 60 records

4.5 Experiment 4

Since the angular resolution and the resolution along the range axis are adversely affected by both larger range distances and poorer SNR, a better ensemble average is obviously needed. The objective of experiment 4 was to note the improvements in resolution as the number of sample records is steadily increased. To do this, the angular resolution of signals with SNR values of 10dB, 6dB, and 3dB was then obtained as a function of the amounts of records used in the ensemble average, as shown in Figure 4.8.

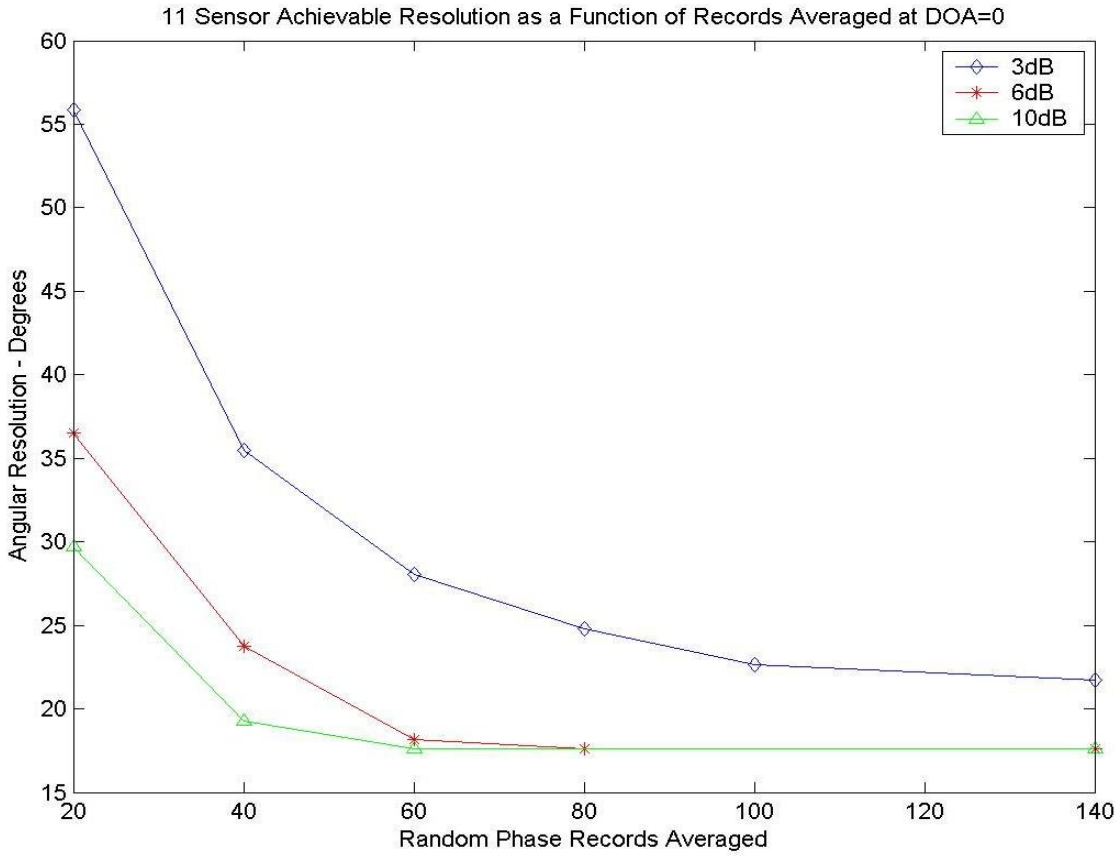

Figure 4.8 – Effect of increasing the number of records used in the ensemble average

This plot suggests that using 100 records or more will especially be important to the sensor data resolution of signals with an SNR value around 3dB. The data taken at 6dB and 10dB indicate that fewer records are needed to increase the resolution notably, but it also seems that a noise resolution limit for this small sensor configuration is met at 17.8°. To increase the possible resolution in DOA and range, larger sensor arrays are needed.

4.6 Experiment 5

For experiment 5, an increase in sensors is seen as another possible method of resolution enhancement. In addition, a longer aperture length will also allow a much deeper near field range. Signals were then simulated from an ensemble average of 140 sample records at a SNR value of 10dB, 6dB, and 3dB. The size of the sensor array was varied using 11 -51 sensors, producing the data set in Figure 4.8.

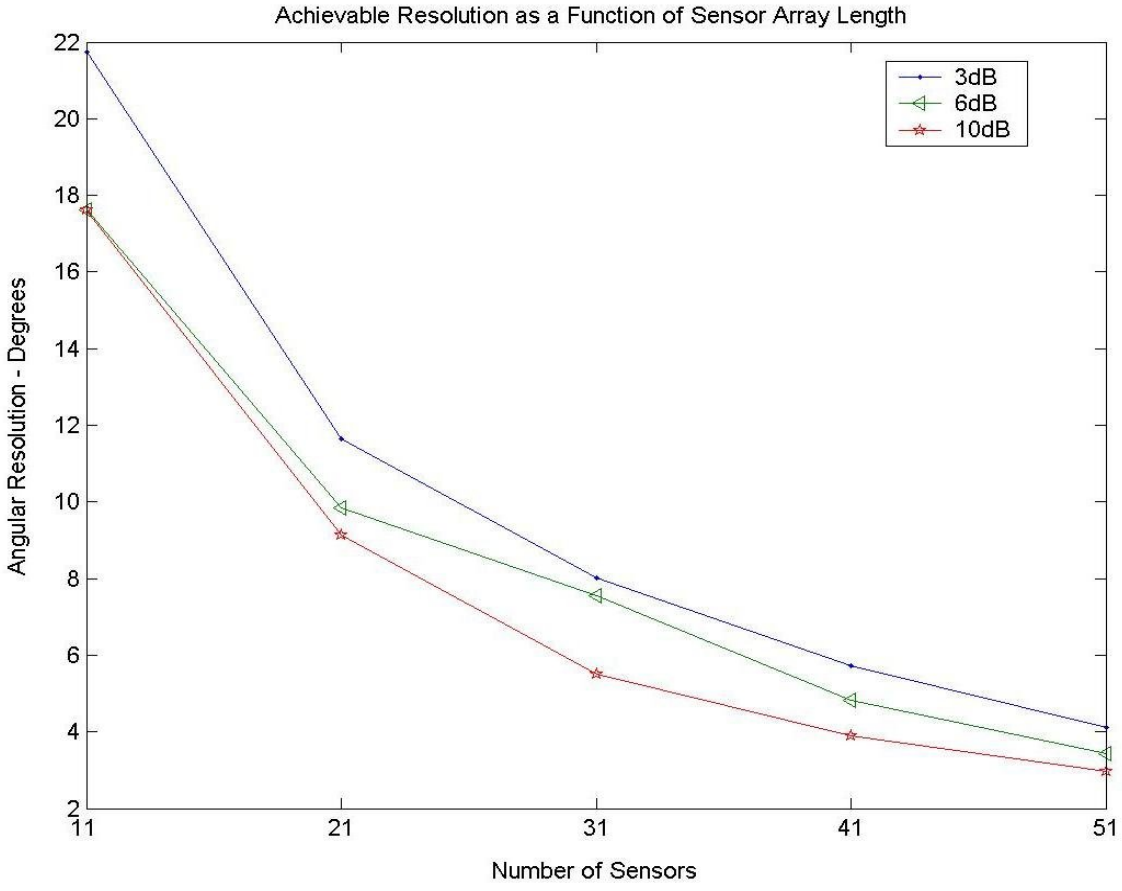

Figure 4.9 – Resolution of sources as the number of sensors in the array are increased

The information given in Figure 4.8 proves that resolution is significantly enhanced while the number of sensor elements is increased. This also provides proof that a near field MVDR method can excel at identification of noisy source distributions and lead to effective source intensity reconstructions as well.

4.7 Experiment 6

The near field source localization work of Grosicki et al. was reviewed in this thesis due to its successful use of a desirable Fresnel approximation. The Grosicki et al. paper also ensured accuracy and prevented phase ambiguities by assuming $m \leq p$ for a $2p+1$ element sensor array, where m is the number of localized sources. To see if the assumption of Grosicki et al. should also be honored by the MVDR method of the thesis, an evaluation of this limitation using the two parameter source localization technique is needed. To test this, equally spaced sources were simulated along a source line in front of an 11 sensor array with $\lambda/4$ interelement spacing. After some trial and error, seven sources were simulated over a field of view of 3λ at positions shown in Figure 4.10.

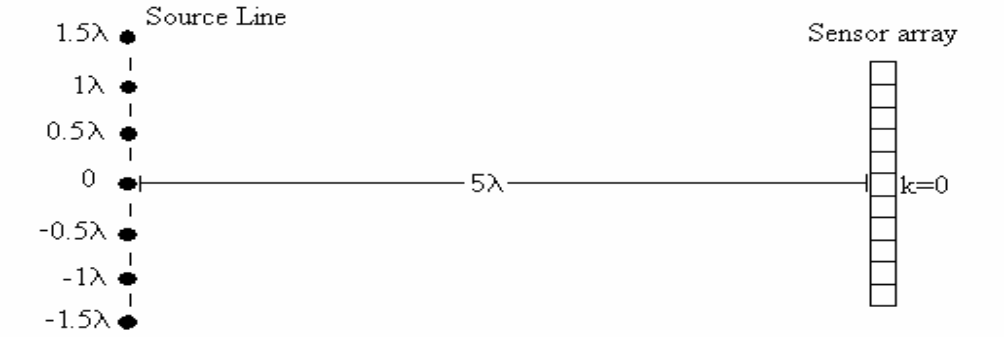

Figure 4.10 – Geometry of the simulated sources for Experiment 6

These sources were then successfully localized as shown in Figure 4.11 using 1000 ensemble average records. The results clearly indicate that this method can resolve more sources than the approach of Grosicki et al. Please note that the peak at 0 radians only looks broader than the rest because of the log units used in the plot.

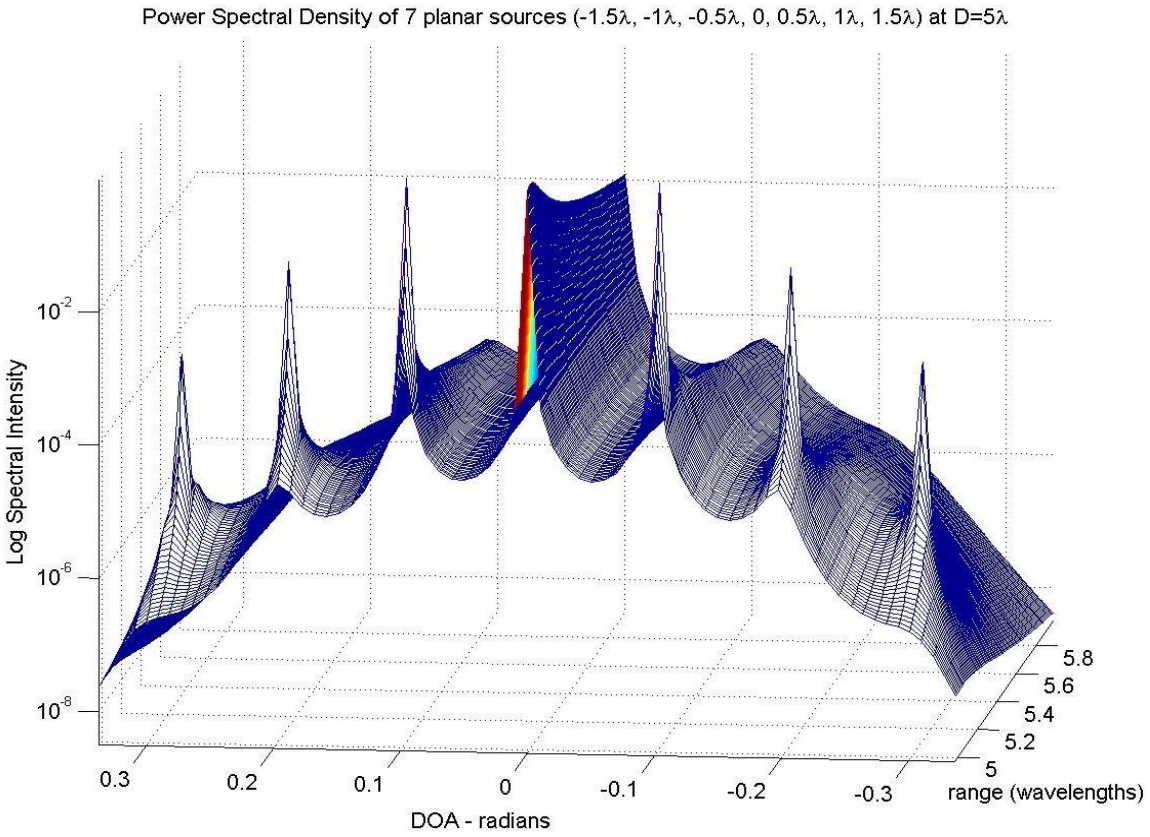

Figure 4.11 – Spatial frequency peaks of 7 sources from 1000 records in Log intensity units

4.8 Near Field Delay and Sum Beamformer Data

To gauge the usefulness of the previous data taken by the Near-Field MVDR method, a simpler method was attempted in a data comparison effort. A simple *delay and sum* beamforming method was implemented to provide this comparison. A traditional delay and sum beamformer identifies the source DOA of far field signals by totaling the signals from each sensor when the signal is delayed by a certain phase:

$$X_{Delay+Sum}(\theta) = \sum_{k=-p}^{p} x_{input} \cdot \exp\left(j \frac{2\pi}{\lambda} kd \sin\theta \right) \qquad for \quad -p \le k \le p \tag{4.1}$$

Delay and sum (4.1) does not use the correlation matrix like a MVDR filter, but produces peaks when the phase product between the signal and steering vector produces a maximum. If d is measured in wavelength units, we can assume λ=1 in (4.1). The only drawback to the function is that excessive oversampling is needed to get a precise response in many far field cases. To reconfigure delay and sum for near field sources and index the sensors as $-p \le k \le p$, the following expression involving range and DOA may be used:

$$X_{Delay+Sum}(\theta, r) = \sum_{k=-p}^{p} x_{input} \cdot \exp\left(j \frac{2\pi}{\lambda} \sqrt{r^2 + k^2 d^2 - 2kd\cos\theta} \right) \tag{4.2}$$

The square root in (4.2) is a geometrically derived expression for the diagonal distance from the source to each k-indexed sensor. Several results were then derived with this equation without noise using similar array sizes, ranges, and DOA measurements to the MVDR data. This data is posted in Table 4.1 and supported by a discussion of the results.

Table 4.1 – Resolution Comparison of 'Delay and Sum' and Near Field MDVR Method

Range from 11 Element Sensor Array	Delay and Sum Resolution (radians)	MVDR Resolution (radians)
1λ	0.795	0.00031
1.5λ	1.10	0.0003
Range from 21 Element Sensor Array	Delay and Sum Resolution (radians)	MVDR Resolution (radians)
1λ	0.622	0.00018
2λ	0.827 (DOA = 0°) 0.873 (DOA = 30°)	0.00018
3λ	1.14 (DOA = 0°)	0.0002

The spatial frequency peaks of the Delay and Sum method for 11 and 21 sensors that were generated within a 1λ range were distinct but had large sidelobes. As the Delay and Sum measurements of both sensor arrays were attempted at slightly larger ranges, the pair of peaks increase in width at an exponential rate. As a result, increases in range beyond 1.5λ for the 11 sensor array, and 3λ for the 21 sensor array, lead to inconclusive Delay and Sum measurements. An example of the near field delay and sum plots used in these calculations is in Figure 4.12. The results posted in Table 4.1 and this discussion show that accuracy and resolution are faulty in this implementation of the Delay and Sum method, and that the range limitations are an issue as well. This also establishes why there is a credible need for precise peak results from a method like the Near-Field MVDR routine that can be used more effectively.

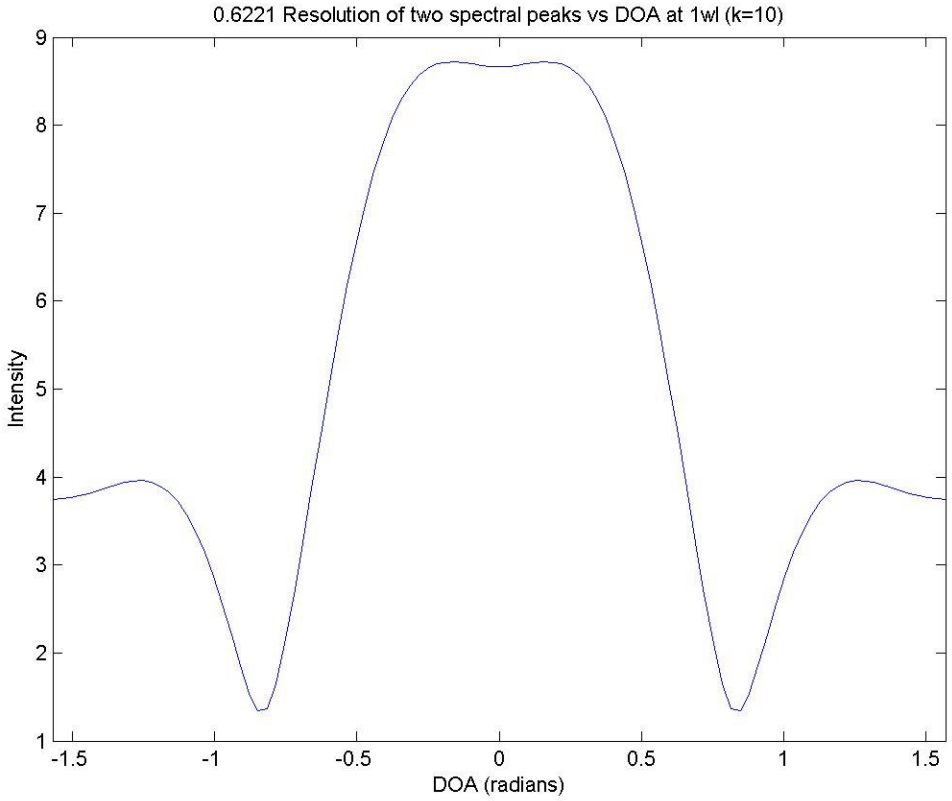

Figure 4.12 – Near field delay and sum beamformer output example

Chapter 5

Conclusion

Through the course of this research, a new algorithm was developed to perform high resolution spectral analysis of source points in the near field. The need for effective field measurement algorithms in high frequency concealed weapon detection has been established. Several previous methods and procedures have been outlined, along with their groundbreaking results and restrictions. This thesis then outlined a desired 2D localization method based on a MVDR routine that calculates filter responses along range and DOA axes. This method was tested with signals of varying noise and direction, but continued to show promise in simulations. Simulations were able to predict limitations to resolution as a result of sensor size and distance from the array. Sources that are close to the array were much easier to resolve along the range axis than those placed towards the far field threshold. Direction of arrival resolution was maximized by both increasing the record samples used to calculate the ensemble average, and increasing the number of sensor elements to enhance sensitivity. Some of the background literature that has been analyzed in this thesis has shown that there are still more ways of increasing the efficiency and sensitivity of methods such as this.

In future studies, one of the first directions for research with a MVDR algorithm would be testing with actual data. If output from a uniform linear array of known size is available, it would be desirable to see how well this method can resolve actual data. This

could be attempted with lines of horizontal data initially, and then modified into a two dimensional method. In two dimensions, the algorithm would need to allow measurement of sources by horizontal DOA, vertical pitch angle, and by their approximate range. In order for this to be possible, a method must be coupled with the MVDR filter output to correctly identify the intensities of the localized field sources. This could be achieved by such means as an eigenspace solution, least squares routine, or a set of optimization commands. Another challenge that may be presented in actual data is obtaining desired results despite hardware limitations, since high frequency sources have brief periods.

A second direction for accomplishment in an MVDR method would be to apply it to wideband data. There are several current methods for wideband data analysis, and research such as that presented by J. C. Chen et al. provides a catalyst for weapon detection using wideband localization of high frequency sources (J. C. Chen et al., 2002). Wideband methods have already shown resolution improvements in their millimeter-wave scanning portal technology as well (Sheen et al., 2001). Since certain terahertz frequencies would aid detector units in automatic identification of concealed explosive devices, a distinct wideband analysis would be a useful tool.

Appendix 1

Table of Abbreviations

CWD	Concealed Weapon Detection
dB	Decibels
DOA	Direction of Arrival
GHz	Gigahertz
MUSIC	Multiple Signal Classification
MVDR	Minimum Variance Distortionless Response
PSD	Power Spectral Density, also referred to as the 'Spectrum' of a signal
RMSE	Root Mean Square Error
SNR	Signal to Noise Ratio
THz	Terahertz
THz-TDS	Terahertz Time-Domain Spectroscopy
UML	Unconditional Maximum Likelihood

Appendix 2

MATLAB Source Code for Correlative Interferometry

```
function thzImage(xv,ex,yv,snr)
% Written by Joseph Handfield ~ongoing revisions 6/12/06
%
% This function calculates an array of spatial correlations of the sensed field
% using an appended array (first half of columns are real parts, others are
% imaginary). It also calculates a theoretical correlation using the
% solution to its integral. The output is an intensity array indicating the
% location of the sources from the least squares computation of both
% correlations.
%
% thzImage uses inputs:
% yv = Array of sensor locations along the sensing line, less than 1/2
%      wavelength-units is the average spacing).
%      * y = linspace(0,3,10) is an example of spacing
%
% xv = Source phasor locations (the distance from 0 (LHS) for electric field points)
%
% ex = Electric field intensities corresponding to xv positions
% ** intensities in ex must correspond with the right position in array xv
%
% User is prompted for:
% 'dv'- distance from source to sensing line.
% 'xn'- number of positions along the source line.
% 'stepSize' - number of random phase samples to accumulate each time before
%   calculating the reconstruction and accuracy.
%
% Optional parameters:
% snr = signat to noise ratio in decibels (SNR = 10*log(signal/noise variance)
% x0- is the minimum starting point (greater than 0) for least squares
% xmax- is the source line width to be correlated
%      (set to the size of the sensing array if no value is entered)
% omega - radian frequency of the incoming waves, set to 2*pi THz for now
%_____________________________________________________________________

% If the program lacks sufficient information, this line will exit.
```

```
if nargin < 3, error('Not enough input arguments.'); end

% Note: dv must be < twice the square of the aperture width over lambda
% freq = input('What field frequency would you like to use, in THz units? ');
disp(' ');
freq = 10^12;
omega = freq * 2 * pi;
sy = size(yv,2);
sx = size(xv,2);

% This identifies the source line length
xmax = input(['What is the end to end span (width) of the source line? ']);
if isempty(xmax), error('No source line span! Shutting down'); end
% Entering a neg or 0 will use the apeture width as a failsafe.
if xmax <= 0
   disp(' ');
   disp('The aperture width will be used.');
   xmax = max(yv);
end
disp(' ');

% This part identifies the number of Ik's to be solved for by the lsq code
% and the max distance/span of the source field
ms = sy*sy - 1;
msg1 = strcat(['How many Ik values do you wish to solve for if ' ...
   num2str(ms) ' is the maximum? ']);
xn = input(msg1);
if isempty(xn), error('No Ik number, shutting down'); end
compCorr = zeros(sy*sy, xn);
disp(' ');
xvall = linspace(0,xmax,xn); % gives the placement of Ik's in the answer array
SrcInt = zeros(xn,1);     % Now to make sure spacing on source line is ok
for count = 1:sx
   SrcInt(find(xvall == xv(count))) = ex(count);
end
if max(SrcInt) == 0
   xmax = input('Your source field width is incorrect. Enter the new length.');
   if isempty(xmax), error('No source line span! Shutting down'); end
   xvall = linspace(0,xmax,xn);
   for count = 1:sx
      SrcInt(find(xvall == xv(count))) = ex(count);
```

```
   end
end

if nargin > 3   % add some random noise according to the snr term
   xv = xvall;
   noiseVar = max(ex) / 10^(snr/10);
   realnoise = normrnd(0,noiseVar,xn,1);
   randn('state',sum(100*clock));
   imagnoise = normrnd(0,noiseVar,xn,1) * i;
   ex = SrcInt + realnoise + imagnoise;
end

% This part will align the sensor across from the central position
% of the source field. If it is not needed later, discard these lines.
ymin = min(yv);
ymax = max(yv);
if min(yv) ~= 0
   yv = yv - ymin; % used to zero the first entry of the sensing array.
end
apwidth = ymax-ymin;
lomiddle = (xmax/2) - (apwidth/2);
yv = yv + lomiddle;

% Source-Sensing distance note: dv must be <= twice the square of the aperture width.
msg2 = strcat(['Your next input must be <= ' num2str((apwidth^2)*2)]);
disp(msg2);
dv = input('What is the wavelength distance between source and sensing lines? ');
if isempty(dv), error('No source-sensing distance, shutting down'); end

% This calculates the 'Theoretical' Computed Correlation as a distance matrix.
% First, the sampled solution AFC using seriesSamp.m
% I'm using the below step to compute the kernel values for all y value
% combinations. Two arrays of horizontal displacements of each field point
% position from the sensors correlatied are picked by a cyclic order
% (sensors 1,1 to n,n) and put into the kernel (autocorrelation operation).
rowCt = 0;
for J = 1:sy
   karray1 = yv(J) - xvall; % 1st set of sensor-field pt. horizontal displacement
   for H = 1:sy
      rowCt = rowCt + 1;
      karray2 = yv(H) - xvall;  % This produces the 2nd sensor-field pt. set
```

```
        % The next step creates a autocorrelation of the spatially vaying
        % kernel- does not produce phase information well, but abs values ok
%         compCorrSpa(rowCt,:) = kernel(dv, karray1, karray2);

      % ADDED 12/4/06 - New Theoretical Correlations:
      % Integral Solution method, since spatial kernel is not exact
      % - ABS value is equal for both Theoreticals but they have different
      % phase components. This is used for checking the actual correlation.
      % Radial assumption used - produces all source displacements from sensor 1 & 2
      r1 = (dv + karray1.^2 ./(2*dv));
      r2 = (dv + karray2.^2 ./(2*dv));

                % Now to calculate the exponential part that will produce the
                % answer for any Ik's, using the expectation derived integral answer.
      compCorr(rowCt,:) = exp((i*2*pi).*(r2 - r1)) ./ (r2 .* r1);
   end
end % And now in order to have a appended real/imaginary matrix
compCorr2 = cat(1,real(compCorr), imag(compCorr));

% A rank check
if rank(compCorr2) < xn
   disp('Warning! Computed Correlation Matrix is not full rank.');
end

% This is the Theoretical R Correlation, using an array of correctly placed
% phasor values and zeros, and the computed correlation matrix (g's).
% bigRspa =  compCorrSpa * abs(SrcInt).^2;
bigR = compCorr * abs(SrcInt).^2;
bigR2 = cat(1,real(bigR), imag(bigR));

% This is the Actual Field Correlation code. It continues to add records and
% compute average until a suitable number of random variable phases give a
% correlation average close to the theoretical correlation values.

% Instantiate my data-keeping arrays & tracking variables (step size & out)

stepSize = input('How many samples per step?');
if isempty(stepSize), error('No step size! Shutting down'); end
x0 = input('Enter a nonzero starting point for lsq solver, or "" to use zero')
if x0 ~= []
   x0= x0*ones(xn,1);
```

```
end

trial = 1; errSet = []; samp = 10;
while trial == 1
        out = 1; records = [];
   phaseA = []; phases = [];
        cAT = []; phaseAvg = []; errPct = [];
        while out == 1
      fpCorr = []; field = [];
      % Next, I'll calculate randomly phased samples of the source field
      [field, phaseA]= seriesSamp(dv,xv,ex,yv,omega,samp);

      % Now to multiply by a exponential array to sample field over one period
                corr = (field*exp(i*2*pi/samp*(1:samp)));
                % The field conjugates are transposed to facilitate matrix multiplication
                corrConj = ctranspose(field*exp(i*2*pi/samp*(1:samp)));
                % Now, to compute the mean of the 10 samples per period
                corrSquare = 1/samp*(corr*corrConj);
      yl = length(yv);
      fpCorr = reshape(transpose(corrSquare),yl^2,1);
      records = [records fpCorr];
      phases = [phases phaseA];
      p2 = mean(phases,2);
      phaseAvg = [phaseAvg p2];
      dpAvg = mean(records,2);
      recnum = size(records,2);
      if mod(recnum,stepSize) == 0
         disp('Random Phases for each reconstruction component:');
         disp(p2'); % Show me the random phase average at this step
         str1 = strcat([num2str(recnum),' records averaged.']);
         disp(str1);
         if x0 ~= []
            [xAns,RESNORM] = lsqnonneg(compCorr2,[real(dpAvg); imag(dpAvg)] ,x0)
         else
            [xAns,RESNORM] = lsqnonneg(compCorr2,[real(dpAvg); imag(dpAvg)])
         end
         % this threshold may need correction for good error analysis
         noiseThr = xAns > 0.5*max(xAns);
         hiFreq = xAns(noiseThr);
         div = sum(SrcInt.^2);
```

```
        errAvg = sum(abs(xAns - SrcInt.^2)) / div *100; % use xn to avg over all IK's
        errPct = [errPct errAvg];
        disp(['Percent error divided by ' num2str(div)]); disp(errAvg);

        % many conditions can be used here to adjust when the random phase
        % iterations can be stopped
        if mod(recnum,200) == 0 % errAvg < 10
           figure;
           plot(errPct);
           out = input('If you would like to sample again type 1:');
        end
      end
      if out ~= 1
        disp('Records finished. Press a button to continue');
        pause;
      end
        end
   errSet = [errSet errPct'];
   trial = input('Another record set to find best error cutoff? 1=yes');
end
dpEstim = cat(1,real(dpAvg), imag(dpAvg));
phaseAvg = mean(phases,2);

if nargin > 5 % Execute a 'check' - Match lsq computations and theoretical data
        disp('');
        disp('Theoretical Solution Check');
        sol1= compCorr2*x2;
        figure;
        plot([abs(bigR) sol1]); % Plot of the (solution x compCorr) versus theoretical
        legend('Theoretical','LSQ Solution');
   title('Theoretical Correlation Vector vs. LSQ Solution');
        ylabel('Correlation Value');
        xlabel('Row (Correlations from 1,1 to n,n)');

        if norm(abs(sol1 - timeAvg2)) > max(timeAvg2)
      disp('This solution is not correct (paused)');
      pause;
        else
      disp('Checks out ok!')
        end
disp('End of Run');    end
```

```
function [nv1,nv2] = seriesSamp(d,x,ex,y,f12,samp)
% written by Joseph Handfield 5/28/06
%
% This function inputs:
% d = the distance value between sensor and source positions
% y = sensor location/separation in wavelengths (also gives # of sensors)
% f12 = frequency of THz waves being examined in radians
% x = wavelength-unit position of x (for example, at 1.3 wavelengths)
% ex = Source phasor coefficients at x position(s)
% samp = number of samples summed throughout the period interval
%
% Other important data:
% Phase = The phase data kept from each sample in units of pi [-1:1]
% (has rows = # of field pts, columns = # of samples)
%
% Output is a randomly phased sample of the source field that is generated
% using the field equation. This simulation of sensor input will be used
% multiple times in the main program to calculate samples that will be be
% ensemble averaged and correlated. The correlation matrix will then be used
% to calculate a reconstruction of the sources.
%_____________________________________________________________________

per = 2*pi/f12;
ymax = length(y);
xmax = length(x);

% pick random phases to use depending on # of points along the source line
phase = (rand(xmax,1)*2 - 1) * pi;

% First the source-sensor radii and the amplitude part must be generated
% to be ymax x xmax to make vector math work.
rad = (d + (repmat(y',[1 xmax]) - repmat(x,[ymax 1])).^2/(2*d));
amp = repmat(ex,[ymax 1]) ./ rad;

% Now the first half of the field expression is produced by multiplying in
% the radial part and the random phases
p1 = amp .* exp(-i*f12*per*rad) .* exp(i*repmat(phase',[ymax 1]));

% This sums up the multi-phased field parts to return the field
nv1 = sum(p1,2);
nv2 = phase;
```

Appendix 3

MATLAB Source Code for Near Field MVDR Method

```
function fresnel(ks, doa)
%
% by Joseph Handfield
% This function calculates near field source fields and inputs the field
% into the Capon function. The DOA, range and intensity of each sensed
% source is returned to this function for MSE analysis with the simulated
% input.
%_____________________________________________________________________
_

dataType = 1; % 1 = Actual Correlation, 2 = Theoretical Correlation (not used)
msg2 = strcat(['Your sensor source D must be <= ' num2str(2*(ks/2)^2) 'wl.']);
disp(msg2);

% The following line can locate the point sources of the test signal along
% an arc of fixed range equal to sfnd(2). Otherwise the sources are located
% along a parallel source plane/line at a distance away determined by sfnd(2).
arc = 0; % input('Fixed range mode for test signal? 1=Yes:');
% sfnd will be a 1 X 2 array of system parameters
sfnd = input('Enter source field width and distance from sensor to source line.');

% loc will be n wide depending on number of sources
loc = input('Enter source locations in array form.');
% The next step will translate the test source locations if a certain DOA is desired
loc = loc + sfnd(2)*tan(doa)
if isempty(loc), error('No location data'); end
% if any(abs(loc) > sfnd(1)/2), error('Need a wider source field'); end

% If simulating non unity intensities for the sources, uncomment next
% line and remove []
val = [1/2 1 1 1/2]; % input('Enter the respective source intensities.');
sources = length(loc); % How many source points are being simulated
if isempty(val) || (length(val) ~= length(loc))
   val = ones(1,sources);
end
```

```
index = -ks:ks;
snsrs = length(index);
phases2 = [];
sensArray = [];
senstotal = 0;
covSum = zeros(snsrs);
rate = zeros(snsrs,sources);
sens = zeros(snsrs,sources);

angleA = atan(loc./sfnd(2))
% The following lines are true for angles that pertain to source line spacing
if arc == 1
   % Lock in broadside distance from sensor to source line sfnd(2) = range
   rate = pi./(16*sfnd(2))*(index').^2*(cos(angleA)).^2 ;
else
   % Normal mode : cos(theta)/sfnd(2) = stretching radius along source line
   rate = pi./(16*sfnd(2))*(index').^2*(cos(angleA)).^3 ;
end
noisy = input('Enter SNR for additive noise, or enter _ for no noise:');
records = 140; %input('Number of records to average?');

% Now to generate samples every 1/10 of a period
timeSamp = exp(i*2*pi/10*(1:10));
if dataType == 1
        for p= 1:records
      phases = [];
      sens = 0;
      for u = 1:sources
         % Separate random phases will be used to 'unlock' simulated sources
         rphase = (rand(1)*2 - 1) * pi;
         part = exp(i*(-pi/2*sin(angleA(u))*index' + rate(:,u)));
         % In the next step, a random phase and time samples are
         % generated for the source signal making 'sens' an array
         % that is # of sensors -by- 10 time samples
         npart = part*timeSamp*exp(i*rphase)*val(u);
         if isempty(noisy) ~= 1
            npart = addNoise(npart,[snsrs 10],noisy);
         end
         sens = sens + npart;
         % Extra sources are added on with different phases
```

```
      phases = [phases rphase];
    end
    corrAvg = 0;
    % Now to time average the correlation of each time sample:
    for ts = 1:10
      corrAvg = corrAvg + sens(:,ts)*ctranspose(sens(:,ts));
    end
    % Now, to time average the sum of the correlations:
    covSum = covSum + corrAvg/10;
    phases2 = [phases2; phases];
      end
  % Now, to ensemble average the sum of the time correlations at random phases:
  covFinal = covSum/records;
end

% Now to calculate the Capon weights and frequency matrix
srcSep = input('What is the distance between positions on the source line?');

% Capon2 takes the correlation matrix and the last sensor output over time
fresp = capon2(index,sens,sfnd,covFinal,srcSep);

if fresp ~= 0
      % These lines produce a crude source line reconstruction, so
      % errors can be computed.
      spos = sfnd(1)/srcSep;
      pvals = length(loc);
      srcLine = zeros(spos,1);
      spacing = (0:spos)*srcSep - sfnd(1)/2;
      for yval = 1:pvals
    p = find(spacing == loc(yval));
    srcLine(p) = val(yval);
    p=0;
      end
      avals = size(fresp,1);
      reconst = zeros(spos,1);
      for ansval = 1:avals
    resp = find(spacing == sfnd(2)*tan(fresp(ansval,1)));
    reconst(resp) = fresp(ansval,3);
      end
      errs = reconst - srcLine;
      disp('The mean squared error is:');
```

```
        meanSqEr = mse(errs)
        disp('end'); disp(' ');
end
prompt1 = input('Another try?');
if prompt1 == 1
   fresnel(ks, doa);
end
```

```
function xout = addNoise(ex,xn,snr)
%
% by Joseph Handfield
% ex = values at xv source positions
% xn = number of reconstruction points & number of time samples
% snr = signal to noise ratio

if nargin < 3, error('Not enough input arguments.'); end
% add some random noise according to the snr term

noiseVar = max(max(abs(ex))) / 10^(snr/10);  % From Reisenfeld & Aboutanios
% The below takes into consideration that the real and imaginary noise proportion is
random
% randPct = rand(1);
noise = sqrt(noiseVar)*randn(xn(1)*2, xn(2));
realnoise = noise(1:xn(1),:);
imagnoise = noise(xn(1)+1:xn(1)*2,:)*i;
xout = ex + realnoise + imagnoise;
```

```
function sArray = capon2(index,sens,sfnd,cov,srcSep)
%
%  Written 5/9/07 by: Joseph Handfield
%  Objective of this function is to execte the Capon Spectral Analysis
%  method on input field data to locate nearfield sources by their
%  incident angle from the central sensor and their radial distance
%  from that sensor. This is done using a manifold array of specially-built
%  frequency filters that combines with the input field signal at various
%  values of theta and r. The ideal value(s) of xc are approximately one.
%_____________________________________________
% 'guess' will tell the algorithm to search the gradient of the spectra for
% a number of peaks
guess = 3; %input('How many sources are you assuming?');
if isempty(guess) || guess == 0, error('No Sources'); end
fov= sfnd(1); distL = sfnd(2);

spos = fov/srcSep;
offs = 0; %input('offset to source line spacing?');
if isempty(offs), offs = 0; end

plotmode = 1; % Enter 1 for mesh/contour plot, 2 for normal 2D plot of a fixed range arc
% Corresponding radii in wavelengths, change the below fraction to modify sampling
distance
if plotmode == 1
   rad = ((0:50)/1000 + 0.98)*sqrt(distL^2 + offs^2);
else
   rad = distL;
end
spacing = (0:spos)*srcSep - fov/2 + offs;
% thetas is set to angles that pertain to the spacing of the source line
thetas = atan(spacing/distL);

invcov = inv(cov);
counter = 0;
%This is here in case diagonal loading is needed (singular correlation matrix)
if any(invcov) == inf
   while estimate < 0.5e-16
      counter = counter + 1;
      cov = cov + eye(length(cov))*0.2; %Amount added can be adjusted to converge
quicker
      estimate = rcond(cov)
```

```
   end
   invcov = pinv(cov);
end

% The next few lines generate the MVDR (Capon?) spectrum
xc = zeros(length(thetas),length(rad));
minvar = zeros(length(thetas),length(rad));
for a = 1:length(thetas)
   for b = 1:length(rad)
      % These calcultions assume that the sensor spacing is lambda/4
      rate = pi/(16*rad(b))*(cos(thetas(a))*index').^2;
      man = exp(i*(-pi/2*sin(thetas(a))*index' + rate));
      minvar(a,b) =  1/ (ctranspose(man)*invcov*man);
      weights = ctranspose(sens)*(invcov*man*minvar(a,b));
      xc(a,b) = sum(abs(weights));
   end
end

% Sobel operators, to create a gradient plot of the spectra
if plotmode == 1
         B1 = [-1 -2 -1; 0 0 0; 1 2 1];
         B2 = [-1 0 1; -2 0 2; -1 0 1];
         u1 = filter2(B1,abs(xc),'same');
         u2 = filter2(B2,abs(xc),'same');
         gradPlot = abs(u1) + abs(u2);

         disp('The Capon Matrix has solution(s) of:');
         % Acccording to value in guess, this picks the maximum valued Capon peaks
         % this was changed to locate all peaks when some may be many orders of
magnitude higher
         temp = log(abs(xc));
   argBkgd = median(median(temp));
         sxc = size(xc);
         aset = [];
         p=0; niter = 0;
         manA = [];

         while p ~= guess
      niter = niter + 1;
      soln = max(max(temp));
      [a,b] = find(temp == soln);
```

```
    if a ~= sxc(1)
       rp = gradPlot(a,b) < 0.5*gradPlot(a+1,b);
    else rp = 0; end
    if a > 1
       lp = gradPlot(a,b) < 0.5*gradPlot(a-1,b);
    else lp = 0; end
    if b ~= sxc(2)
       up = gradPlot(a,b) < 0.5*gradPlot(a,b+1);
    else up = 0; end
    if b > 1
       dp = gradPlot(a,b) < 0.5*gradPlot(a,b-1);
    else dp = 0; end
    if (rp && lp) && (up && dp)
       soln
       disp(['at theta = ' num2str(thetas(a)) ...
          ', and at a radius = ' num2str(rad(b))]);
       rateA = pi/(16*rad(b))*(cos(thetas(a))*index').^2;
       manA = [manA exp(i*(-pi/2*sin(thetas(a))*index' + rate))];
       p = p+1;
       % If the solution positions are to be recorded
       aset = [aset; thetas(a) rad(b) 0];
    end
    if niter > 3*guess
       disp('Valid Capon solutions are found');
       p=guess;
    end
    temp(a,b) = argBkgd; % Reduce the solution peak so others can be located
       end
       pic = input('Would you like to create a mesh plot? Enter title.');
       if isempty(pic) == 1
    % do nothing
       else
%      figure;
%      logMVDR = log(abs(xc));
%      mesh(rad,thetas,logMVDR);
%      axis tight;
%      ylabel('DOA - radians');
%      xlabel('range (wavelengths)');
%      zlabel('Log Spectral Intensity');
%      graph = strcat(['MVDR Filter Response ' pic]);
%      title(graph);
```

```
      % For Power Spectral Estimator (denominator of Capon solution)
      figure;
      mesh(rad,thetas,abs(minvar));
      ylabel('DOA - radians');
      xlabel('range (wavelengths)');
      zlabel('Spectral Intensity');
      axis tight;
      graph2 = strcat(['Power Spectral Density of ' pic]);
      title(graph2);
%       figure;
%       maxLog = fix(max(max(logMVDR)));
%       levels = (-10:0) + maxLog;
%       [cs, h]= contourf(rad,thetas,logMVDR,levels); clabel(cs,h);

        %    in2 = input('To save jpeg, type 1');
        %    if in2 == 1
        %       print(gcf, '-djpeg', pic);
        %       clear temp;
        %       save(pic);
        %    end
        end

        % Gaussian elimination division to find intensities of field points
        if length(manA) ~= 0
      intens = max(abs(sens'))/manA'
      aset(:,3) = intens';
        end
        sArray = aset;
else
   figure;
   plot(thetas,log(abs(xc)));
   xlabel('DOA - radians');
   ylabel('Log Spectral Intensity');
   sArray = 0;
end
```

Appendix 3

MATLAB Source Code for Delay and Sum Method

```
function nearDelaySum

% delay & sum for spherical wavefront
C=3e8; % EM wave velocity
j=sqrt(-1);

N=11; % number of (odd) sensors, modify to desired size
dx= 0.25; % separation between sensors. Assumed wavelength=1.
R= 1; % distance of source from center sensor. qualifies for near field
Theta= pi/6; % angle of arrival of source at center sensor
cent_dist= -dx*(N-1)/2; % distance of leftmost sensor from center to begin with
source_dist= zeros(1,N); % distance of each sensor from source
for n=1:N,
    source_dist(n)=sqrt(R^2+cent_dist^2-2*cent_dist*cos(Theta));
    cent_dist=cent_dist+dx;
end % source distance generated
% now generate phasors
phasors=exp(-j*2*pi*source_dist); % assuming lambda=1
% now test output delay and sum as a function of angle
target_dist= zeros(1,N); %distance of each sensor from assumed target
del_sum=zeros(size(-pi/4:pi/20:pi/4)); %assuming angles from -pi/4 wavelength to pi/4
i=0;
for theta=0:pi/100:pi,
    i=i+1;
    cent_dist= -dx*(N-1)/2; % distance of leftmost sensor from center to begin with
    for n=1:N,
        target_dist(n)=sqrt(R^2+cent_dist^2-2*cent_dist*cos(theta));
        cent_dist=cent_dist+dx;
    end % distance to assumed target generated
    % generate corresponding phasors for delay and sum
    phasors_del=exp(j*2*pi*target_dist);
    % generate delay and sum magnitudes for given r
    del_sum(i)=abs(sum(phasors.*phasors_del));
end
figure;plot(0:pi/100:pi,del_sum);
```

References

J. G. Arceo-Olague, D. H. Covarrubias-Rosales, and J. M. Luna-Rivera, 'Efficiency Evaluation of the Unconditional Maximum Likelihood Estimator for Near-Field DOA Estimation,' *ETRI Journal*, Vol. 28, No. 6, 761-9, (December 2006).

'Assessment of Millimeter-Wave and Terahertz Technology for Detection and Identification of Concealed Explosives and Weapons,' Committee on Assessment of Security Technologies for Transportation - National Research Council, National Academies Press, Washington, D.C., http://www.nap.edu/catalog/11826.html, (2007).

G. R. Benitz, 'High-Definition Vector Imaging,' *Lincoln Laboratory Journal*, Vol. 10, No. 2, 147-170 (1997).

J. Capon, "High-Resolution Frequency-Wavenumber Spectrum Analysis," *Proceedings of the IEEE*, Vol. 57, No. 8, pp. 1408–1418, (August 1969).

H. Chen, S. Lee, R. M. Rao, M. Slamani, P. K. Varshney, "Imaging for Concealed Weapon Detection," *IEEE Signal Processing Magazine,* 52-61 (March 2005).

J. C. Chen, R. E. Hudson, and K. Yao, 'Maximum-Likelihood Source Localization and Unknown Sensor Location Estimation for Wideband Signals in the Near-Field,' *IEEE Transactions on Signal Processing*, Vol. 50, No. 8, 1843-1854 (August 2002).

M. H. Cohen, "Introduction to very long baseline interferometry," *Proceedings of the IEEE*, vol. 61, 1192-97, (1973).

T. Dorney, J. Johnson, D. Mittleman, R. Baraniuk, "Imaging with Terahertz Pulses," Applications of Digital Image Processing, *Proceedings of SPIE*, **4115**, 689-699 (2000).

J. F. Federici, D. Gary, R. Barat, D. Zimdars, "Terahertz Imaging Using an Interferometric Array," *Proceedings of SPIE*, Vol. 5790, 11-18 (2005).

J. F. Federici, B. Schulkin, F. Huang, D. Gary, R. Barat, F. Oliveira and D. Zimdars, "THz imaging and sensing for security applications - explosives, weapons and drugs," *Semiconductor Science & Technology*, Institute of Physics Publishing, **20**, S266-S280 (2005).

E. Grosicki, K. Abed-Meraim, and Y. Hua 'A Weighted Linear Prediction Method for Near-Field Source Localization,' *IEEE Transactions on Signal Processing*, Vol. 53, No. 10, 3651-3660 (Oct. 2005).

E. Hecht, Optics. Third Ed. Reading, MA: Addison-Wesley, (1998).

B. B. Hu and M. C. Nuss, "Imaging with terahertz waves," *Optics Letters*, **20**, pp. 1716–1718 (1995).

Y. Jiang, P. Stoica, Z. Wang, J. Li, 'Capon Beamforming In the Presence of Steering Vector Errors and Coherent Signals,' *Annual Workshop on Adaptive Sensor Array Processing* (*ASAP*), MIT Lincoln Laboratory, Lexington, MA, (March 11-13, 2003).

J. L. Johnson, T. Dorney, D. Mittleman, 'Background-Free THz Imaging Using Interferometric Tomography,' *CLEO Conference Proceedings*, 526 (2000).

S. M. Kay, S. L. Marple, "Spectral Analysis – A Modern Perspective," *Proceedings of the IEEE*, Vol. 69, No. 11, (1981).

D. L. Marks, R. A. Stack, D. J. Brady, "Three-Dimensional Coherence Imaging in the Fresnel Domain," *Applied Optics*, Vol. 38, No. 8, (1999).

C. L. Nikias and J. M. Mendel, 'Signal Processing with Higher Order Spectra,' *IEEE Signal Processing Magazine*, 10-37 (July 1993).

R. M. Rao, B. Himed, 'Correlative Interferometric Imaging of Extended Objects for Near Field Arrays', *IEEE International Workshop on Computational Advances in Multi-Sensor Adaptive Processing*, Puerto Vallarta, 32-35, (Dec. 2005).

D. M. Sheen, D. L. McMakin, and T. E. Hall, 'Three-Dimensional Millimeter-Wave Imaging for Concealed Weapon Detection,' *IEEE Transactions on Microwave Theory and Techniques*, Vol. 49, No. 9, 1581-1592 (September 2001).

P. Stoica and R. Moses, *Introduction to Spectral Analysis*. Upper Saddle River, NJ: Prentice Hall, (1997).

C. Vaidyanathan and K. M. Buckley, 'Performance Analysis of the MVDR Spatial Spectrum Estimator,' *IEEE Transactions on Signal Processing*, Vol. 43, No. 6, 1427-1437 (June 1995).

K. P. Walsh, B. Schulkin, D. Gary, J. F. Federici, R. Barat, D. Zimdars, 'Terahertz Near-Field Interferometric and Synthetic Aperture Imaging,' *Proceedings of SPIE*, Vol. 5411, 9-17, (2004).

F. Zernike, "The Concept of Degree of Coherence and its Application to Optical Problems," *Selected Papers on Interferometry* (Ed: P. Hariharan), SPIE Optical Engineering Press, **MS28**, 33-40 (1990).

D. Zimdars, 'High Speed Terahertz Reflection Imaging,' *Proceedings of SPIE*, Vol. 5692, 255-9 (2005).